



بسم الله الرحمن الرحيم

Sudan University of Science and Technology



Faculty of Engineering

Aeronautical Engineering Department

Control a Morphing Trailing Edge

—Thesis Submitted in Partial Fulfillment of the Requirements for the
Degree of Bachelor of Science. (BSc Honor)

By:

1. Doaa Mohamed Ali Ahmed
2. Esraa Adil Mohamed Al-shikh

Supervised By:

Dr. Osman Emam

October,2016

الآية

بِسْمِ اللَّهِ الرَّحْمَنِ الرَّحِيمِ

(يَا مَعْشَرَ الْجِنَّ وَالْإِنْسِ إِنِ اسْتَطَعْتُمْ أَنْ تَنْفُذُوا مِنْ أَقْطَارِ السَّمَاوَاتِ وَالْأَرْضِ
فَانْفُذُوا ۚ لَا تَنْفُذُونَ إِلَّا بِسُلْطَانٍ)

سورة الرحمن الآية (33)

Abstract

Aircraft designers have been focusing on improving the aircraft flight efficiency, and especially airline companies are anxious to improve the commercial aircraft efficiency nowadays. Usually aircraft wings are designed to be most efficient at cruising flight, but suffer performance penalties under other conditions, such as taking off, landing and controlling flight attitude.

Morphing technology, inspired by bird flight enables an aircraft to adapt its shape to enhance mission performance and optimize flight attitude controlling efficiency.

This work is aimed at controlling the airfoil camber at the wing trailing edge by producing a smoothed morphed flap upon activation of the smart material (SMA elements), substituting the traditional split hinge flap of the civil regional transportation aircraft.

التجريد

تصمم الطائرات غالبا لتكون أكثر فعالية أثناء تحليقها في الهواء بينما تكون أقل فعالية في مراحل الهبوط والإقلاع ، تعمل شركات الطيران في الأونة الأخيرة على حل هذه المشكلة بإستخدام تقنية جديدة تجعل الجناح ينحني بدون أن يفصل لزيادة كفاءة الأداء.

يقصد من هذا المشروع التحكم بذيل الجناح بجعله ينحني تحت تأثير تفعيل المعادن الذكية وإستبداله ليحل محل الذيل التقليدي للجناح بالطائرات.

Acknowledgement

We would to thank everyone who contributed in making the project dissertation possible

Our supervisor Dr. Osman Emam for his patient and knowledge....

Our teacher Ms. Raheeg Alamin for her guidance all the path ...

Aviation research Centre for their great help and efforts ...

Dedication

we dedicate our dissertation work to our families and many friends. A special feeling of gratitude to our loving parents who taught us that the best kind of knowledge to have is that which is learned for its own sake and taught us also that even the largest task can be accomplished if it is done one step at a time.

Contents

الآية	I
Abstract	II
التجريد	III
Acknowledgement	IV
Dedication	V
List of figures	VIII
List of tables.....	IX
list of abbreviations.....	X
Symbols.....	XI
Chapter 1: Introduction	1
1.1 Introduction	1
1.2 Problem statement	1
1.3 Proposed solution	1
1.4 Aim and Objectives	2
1.5 Motivation	2
1.6 Methodology	2
1.7 Outline.....	3
Chapter 2: Literature Review	4
2.1 History and Background.....	4
2.2 Morphing technology	5
2.3 Morphing skins.....	11
2.4 Actuation for morphing technique	12
2.5 Morphing Trailing edge	15
2.6 Structural design, calculation and simulation	15
2.7 Control system and methodology.....	21
2.8 Experiments and results	24
Chapter 3: Model Descriptions	29
3.1 Morphing Trailing Edge Wing Model	29

3.2	Shape memory alloys Actuator	32
3.3	ABS Skin.....	33
3.4	Test Result of wind tunnel	35
Chapter 4: Control System For A Morphing Trailing Edge		36
4.1	Control Theory	36
4.2	Types of PID Controllers	38
4.3	Response analyze of the PID controller	42
4.4	Mathematical model of the SMA actuator	43
4.5	Control formula and Simulation approach.....	48
Chapter 5: Result And Discussion		51
5.1	Result Demonstration and Assessment	51
5.2	Evaluation Result	54
Chapter 6: Conclusion And Recommendations.....		55
6.1	Conclusion:.....	55
6.2	Recommendation:.....	56
6.3	Future work:	56
References.....		57
Appendix A: Flowchart of the Heating and Cooling of SMA		
Appendix B: MATLAB M-File		

List of figures

Figure 1: Morphing wing concept.....	6
Figure 2: Types of the morphing	7
Figure 3: wing planform alternation	9
Figure 4: Airfoil profile adjustment.....	10
Figure 5: Out-of-plane transformation of the wing.....	11
Figure 6: Composite plate.....	12
Figure 7: (a) Sketch of the airfoil model (b) 3D model morphing.....	16
Figure 8: The sketch of concentrated forces simplified from aerodynamic loading	17
Figure 9: Sketch of SMA model arranged on a single segment	19
Figure 10: (a) Simulation of deflection upward; (b) Simulation of deflection downward	21
Figure 11: Sketch of measurement and control system	22
Figure 12: The experimental environment and equipment	24
Figure 13: (a) The wingtip displacement of deflection downwards; (b) The wingtip displacement of deflection upwards.....	26
Figure 14: (a) The control effect at 1° ; (b) PWM signal pattern in the control procedure	27
Figure 15: (a) The control effect at 1° ; (b) PWM signal pattern in the control procedure	27
Figure 16: Sketch of integral deflection.....	28
Figure 17: (a) The control effect at -3° of integral deflection upwards (b) The control effect at 3 degrees of integral deflection downwards	28
Figure 18: Clark Y airfoil	29
Figure 19: Side view of the experimental wing model	30
Figure 20: Schematic diagram of the SMA actuators layout (top view)	31
Figure 21: Heating and Cooling of SMA.....	32
Figure 22: Transient and Steady-State Response Analyses	43
Figure 23: Martensite Fraction vs Temperature.....	45
Figure 24: Block diagram of the system under consideration	48
Figure 25: PID Controller block of morphing trailing edge	49
Figure 26: Simulation scheme	50
Figure 27: The time response with I Controller for heating	51
Figure 28: Scope Result for heating.....	51

List of tables

Table 1: Actuation Design Alternatives.....	14
Table 2: Values of concentrated forces.....	18
Table 3:The relationship between e and q	23
Table 4: The response times and the errors between the practical deflection angles and the target angles	26
Table 5: Specifications of nickel titanium (SMA) wire FLEXINOL® wires.....	31
Table 6: trailing edge deflection of the wing panel ith ABS skin.....	35
Table 7: Effects of coefficients	42
Table 8: Effects of each of controller K_p , K_d , and K_i on a closed-loop system	42
Table 9: Characteristic and controller Parameters for heating.....	52
Table 10: Characteristic and controller Parameters for cooling	54

list of abbreviations

ABS	Acrylonitrile butadiene styrene
NASA	national Aeronautics and space Administration
PID	proportional-integral-derivative
SMA	shape memory alloy
UAS	unmanned Aerial system
UAV	unmanned Aerial vehicle

Symbols

A	Axial force (N)
A _f	Austenite finish temperature (°C)
A _s	Austenite start temperature(°C)
e	Control error
E	Young's modulus (Pa)
h	Heat convection coefficient (J.m ⁻² .s ⁻¹ .K ⁻¹)
H	Latent heat (J.kg ⁻¹)
ISMA	Signal input to SMA actuator
KD	Derivative gain
KI	Integral gain
KP	Proportional gain
M _f	Martensite finish temperature (°C)
M _s	Martensite start temperature (°C)
S	Wing planform (m)
S	Control system output
S _{ref}	Control system input
t	Time (s)
T	Temperature (°C)
U	Voltage (V)
u	Input voltage (V)
σ	Stress (Pa)
σ _a	Martensite to austenite transformation stress (Pa)
σ _m	Austenite to martensite transformation stress (Pa)
ε	Strain
ε _i	Initial strain
ε _{ref}	Strain reference trajectory
ξ	Martensite fraction
ξ _a	Martensite to austenite transformation fraction
ξ _m	Austenite to martensite transformation fraction
θ _t	Thermal expansion (N.m)
Ω	Phase transformation contribution factor (Pa)

Chapter 1: Introduction

1.1 Introduction

Morphing is a smooth variation of the geometry or it is the ability to morph or to change the form to undergo transformation, In the field of engineering the word morphing is used when referring to continuous shape change no discrete parts are moved relative to each other, but one entity deforms upon actuation, morphing airfoil concept is meant to replace the traditional flap, ailerons, elevator and rudders in order to improve the aerodynamic efficiency.

For actuation mechanism Shape Memory alloys actuators (SMA) were used to morph the flexible skin (usually made of composite material). SMA is considered ideal for their favourable performance per weight ratio, Shape Memory Alloys are materials regaining its undeformed original shape when heated, after deformation performed at a low temperature. An SMA has two crystalline phases called Martensite and Austenite. In the Martensite phase at a low temperature, the material yielding stress is low and a deformation can be applied with a relatively small applied force. Heating the SMA causes the phase transformation from the Martensite to the Austenite, recovering the deformation and returning to its initial shape, the simulation of the architecture of the SMA elements evaluated with specific Matlab routine.

1.2 Problem statement

The discrete nature of flaps or ailerons on a wing (hinge) cause drag-inducing vortices in the aileron gaps and this contribute to the drag of the aircraft and limiting the performance especially the range and endurance. Conventional control surfaces allow only a limited number of degrees of freedom which constrain the ability to maneuver, the actuation mechanism has a slow response makes a huge burden on the pilot and needs to a great effort from him and still sometimes the flap gets stuck and doesn't work properly,all this leads to more fuel burning and environmental pollution.

1.3 Proposed solution

A morphing trailing edge concept is proposed to replace the traditional flap, ailerons, elevator and rudders in order to improve aerodynamic efficiency by delaying the laminar

transition point, it offers the potential to decrease the fuel burn of aircraft by allowing the wings to dynamically adjust to changing flight conditions.

The morphing trailing edge is expected to achieve Continuous deflection up and down, also the state stability at specific angles is indispensable, the actuation concept relies on a quick-return mechanism of the SMA wire which mainly cause the flap to bend.

1.4 Aim and Objectives

- **Aim**

Modelling a control system that moves a morphing trailing edge of shape memory alloy (SMA) with high accuracy, and reliability.

- **Objectives**

- 1) Study and analysis the SMA actuators and the flexible morphing skin material.
- 2) Explore mathematical models which explain the force, strain of the SMA.
- 3) Derive control laws which achieve desired deflection of morphing trailing edge.
- 4) Simulate the movement of the morphing trailing edge in a Matlab environment.

1.5 Motivation

Wing shape morphing is a very promising area of research, changing the wing shape or geometry for maneuver and general control purposes has a key benefits appears effectively in the low environmental impact.

The goal of developing a morphing wing is that it will be able to accomplish tasks that the conventional wing can not perform, Several researchers are studying the bird flight in order to mimic it on the real aircrafts, nowadays this approach take the interest and directivity of all aircrafts manufactures.

1.6 Methodology

Theoretical and analytical methodology have been used to go through this study, matlab is used for simulation , the SMA thermo-mechanical behaviour has been estimated by means of Liang & Rogers' mathematical model with respect to the SMA wire specification, nickel titanium wire produced by Dynalloy Inc company has been used at the morphing trailing edge model, experimental wind tunnel tests have been carried out by the RMIT university are

considered to significant the constrains of the different conditions and evaluate the life environment.

Control law has been derived to met the requirements of the heating and cooling phase which describe the dynamic of the entire system. The project was adopted in its implementation mainly on the Matlab software program, and a simulation procedure has been used to virtually simulate the SMA actuation and thus the trailing edge deflection.

1.7 Outline

The dissertation contains a five chapters, chapter one is an introductory chapter has the general idea of the project, purpose, and methodology, next chapter covering basically the history and background of the morphing technology, shape memory alloy actuator (SMA) and the critical literature review, chapter three is a description of the model, chapter four shows the model actuation mechanism, control theory and simulation, chapter five consists of the result and the discussion, and chapter six included the conclusion, recommendations, and future work.

Chapter 2: Literature Review

2.1 History and Background

Changing the wing shape or geometry for maneuver and general control purposes has its roots at the very early stage of the modern aviation. The Wright Flyer, the first engine aircraft 1903, enabled roll control by changing the twist angle of its wing, by using cables directly actuated by the pilot. The increasing demand for higher cruise speeds and payloads led to more rigid aircraft structures, unable to change their shape to different aerodynamic conditions. The deployment of conventional flaps or slats on a commercial airplane is the common way to modify the wing geometry (other examples are the variable wing plan geometry on the F14 or the Concorde nose) however, they lead to discontinuities, in turn producing geometry sharpening, aerodynamic efficiency worsening and also noise emissions increase.

The first designs of variable geometry aircraft occurred in the 1930s. In an attempt to improve cruise performance in aircraft by reducing induced drag, global morphing designs such as telescoping or folding wings allowed for changes in aircraft performance to be made before flight. Also during this time, aircraft construction materials transitioned largely from cloth and wood to rigid metal to increase structural stiffness for faster aircraft. Thus, the local morphing concepts pioneered by the Wright brothers were largely eliminated from aircraft as increased flow speeds demanded localized compliance in the form of hinges and pivots that could be blocked by the simplistic actuators of the time. Still, global morphing designs progressed to in-flight adaptation that included sweep, dihedral and folding.

The first modern instance of distributed local morphing in modern aircraft was the Mission Adaptive Wing (MAW), developed in the 1980s as a testbed for a multirole F-111 tactical aircraft requiring supersonic cruise speed and high maneuverability [1]. The aircraft attempted to eliminate the discontinuities due to discrete flaps and hinges by creating a smooth upper surface from composite materials that bent due to actuation. Continuous local morphing was achieved with hydraulic actuators that varied leading and trailing edge camber in flight. The leading edge actuation was a single-span surface, but the trailing edge utilized three span-wise separated panels capable of independent actuation. Additionally, the aircraft could sweep its wings to

achieve global morphing for reduced drag at high cruising speeds. Although it used conventional actuators with a relatively limited number of discrete span-wise sections, the concept demonstrated that span-wise variation of local morphing can reduce loading on the wing, improve ride quality, cruise performance and maneuverability [1].

Starting in the early 1990s, the NASA Aircraft Morphing Program attempted to enable “self-adaptive flight” by integrating novel smart technologies including embedded actuation, sensing, and control logic to improve aircraft efficiency [2]. The program covered a very wide scope, attempting to combine multiple disciplines to perform system studies for identifying component technologies with the highest benefit in a real aircraft. One target capability identified by the program was active flow separation control for a 15 percent decrease in high lift system weight [2]. The result was a focus on “smart materials” to address the multidisciplinary aspect of the program and enable program objectives of active aerodynamic and aeroelastic control.

In a similar fashion, the DARPA/AFRL/NASA Smart Wing program sought to develop and demonstrate the use of “smart” technologies, including smart materials to improve aerodynamic performance, for a transonic military aircraft, operating from 1995 until 2001, the program tested span-wise varying hinge-less “smart” trailing and leading edges compared to conventional control surfaces corresponding to a representative take-off and cruise condition.

2.2 Morphing technology

The definition of morphing is still widely open to interpretation. Derived from the Greek word “morphs” meaning “shape”, morphing in the context of aircraft has commonly been defined as large shape change or more generally as “efficient multipoint adaptability” [2]. The latter definition inherently implies novel mechanisms or materials or a reduction in energy use to differentiate morphing from conventional designs. An even broader definition of “morphing aircraft” also includes other conventional adaptive mechanisms such as slotted flaps, retractable landing gear, variable pitch propellers, and variable sweep.

Although morphing technologies are relatively new as research areas in aerospace, the design of changing wing planforms is as old as motorized flight itself. The pioneers of flight, Orville and Wilbur Wright, were the first to fly a powered heavier-than-air flying machine on 17 December 1903. This machine used flexible wings with pulleys and cables that twisted the wingtips. Back then such an approach was known as wing warping, but it is nowadays referred to

wing morphing, an active structure can be defined as possessing an ability to change shape whilst maintaining a continuous form, whereas a passive structure, such as a hinged aileron, has discrete components which move relative to each other figure(1).

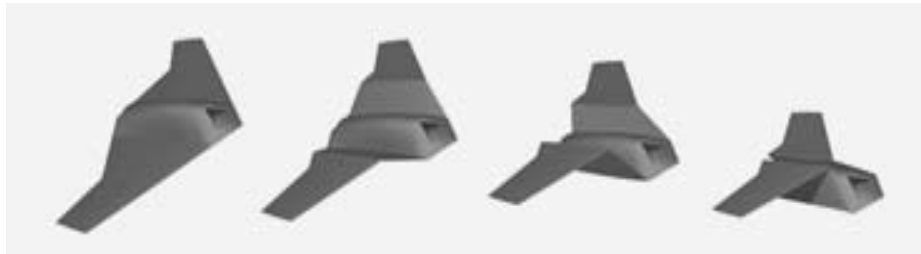


Figure 1: Morphing wing concept.

Wing morphing technology may provide a solution to the aerodynamic predicament as it is capable of enhancing the aerodynamic performance of the UAV by modifying the wing shape when needed. It could be used to improve its loiter time and also reduce the power required. The desired aerodynamic result is then an aircraft that can undergo a large geometry changes to perform efficiently over a variety of flight conditions, necessitating a structural design that is compliant where necessary for shape-change. Still, the structure of the aircraft must support the aerodynamic loads throughout the morphing process and at all flight conditions, necessitating a stiffer structural design and actuators capable of overcoming the aerodynamic loads. Additionally, the weight of the aircraft negatively impacts its performance, penalizing heavy, complex solutions for the actuators and structure. Thus the coupled design of a morphing concept must consider all of these topics concurrently, resulting in many different solutions, varying for different flight regimes.

The wing morphing concepts can be classified into three major types: planform alternation, out-of-plane transformation, and airfoil adjustment Fig(2).

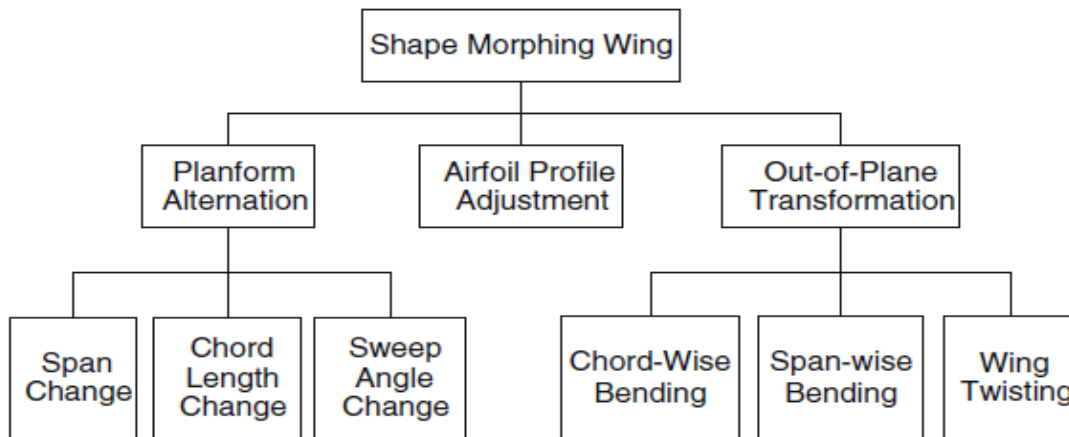


Figure 2: Types of the morphing

Plan form wing alternation

The wing planform can be reconfigured by the resizing of span and chord length, and by changing the sweep angle, as depicted in Fig 3 Combinations of the above are also possible.

(1) Wing span resizing

Telescopic structures have been extensively used for dramatic length change of the wing structure. The morphing wing in the telescopic designs is sectioned longitudinally to form several segments with reducing cross sectional area, such that each segment can be accommodated in the adjacent inner segment with a minimum sliding clearance. Given the required length change, the number of segments can be determined.

A approach to change the wing span uses scissors-like mechanism for the wing-box. Joo et al. studied the optimal location of a distributed network of actuators within a scissor wing-box mechanism, their reconfigurable wing-box was made of four bar mechanisms with rigid links. An experiment was conducted on a single cell linkage by using a pneumatic actuator which was connected to two neighbouring links. An optimization analysis was performed to select the optimal location of actuator placements. Springs were used in their design to account for a stretchable skin, but a parametric study of the compliance was not done.

(2) Chord length change

The chord length of the wing in conventional aircraft is resized by means of leading/trailing edge flaps, which are usually moved by lead and screw actuation systems. Many of these devices are patented and operational. Very few researchers exploited the resizing of the chord length without using such flaps or slats. They used mechanism to change the chord length by means of miniature DC motors and lead screws, they used partial rib structures that could slide through a central slotted box and alter the chord wise position of the leading and trailing edges. The ribs were designed to support the camber bending due to the aerodynamic loads. Rotation of the output motor shaft located at the fuselage was transmitted to the lead screws (attached to the moving ribs) with a lateral rotating rod. The smooth operation of the lead and screw mechanism under transverse aerodynamic loads is questionable. In addition, maintaining the chord-wise bending stiffness of the wing remained a challenge. The application of smart materials, on the other hand, to achieve chord change is one of the least studied methods of wing morphing.

(3) Sweep angle variation

Pivoting of the wing so far has been the method of choice for the sweep change, or even for the shape morphing, implemented in many successful and operational aircraft such as: Bell-X-5, F-111, F-14, and B-1. All of the aerodynamic loads on the wing in those designs are supported by a pivoting mechanism. Such a pivot is complex to build and install. It is heavy and needs elaborate maintenance.

In a rare effort to use smart materials to achieve sweep change, Yu et al [] used shape memory polymer (SMP) for the shear deformation of a scissors mechanism, The scissors mechanism was deformed as a result of the hinge rotation.

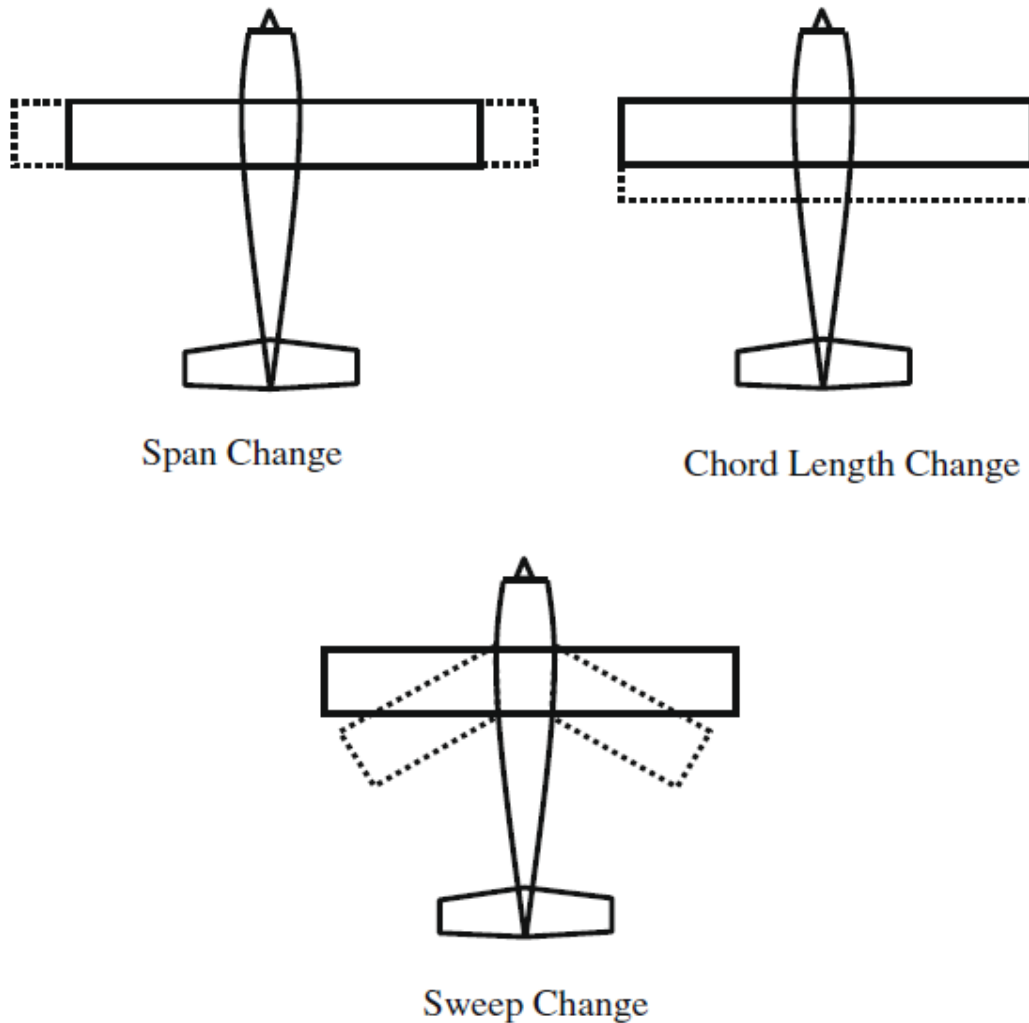


Figure 3: wing planform alternation

Airfoil profile adjustment

Several researchers have explored the ways to alter the aerodynamic properties of the wing by the reshaping of the airfoil profile (without significant change of its camber), to do so the upper and/or lower chamber of the airfoil is changed without major changes of the mean camber line, Fig (4).

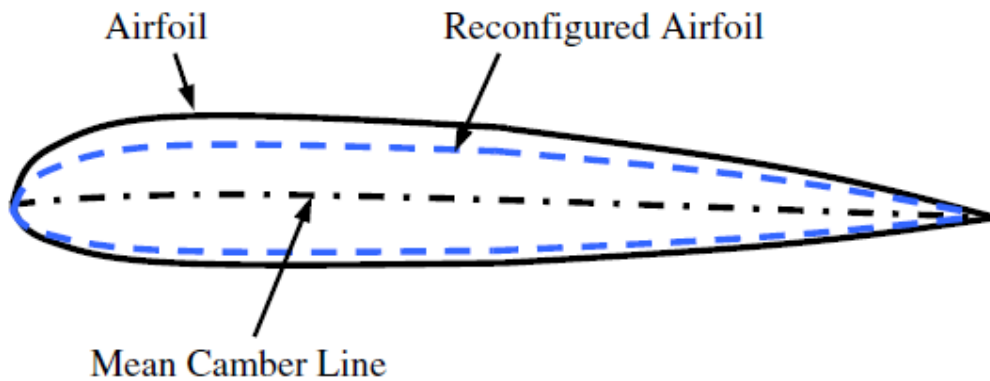


Figure 4: Airfoil profile adjustment.

Variable length trusses were examined by Austin et al. to reshape the airfoil, attached linear displacement actuators inside the wing section in a diagonal manner. The airfoil shape could therefore be modified by the expansion or contraction of the actuators.

The suitability of SMA actuation for morphing of aircraft wing has been first demonstrated by the designs that changed the airfoil profile. A prominent sample is the design by Strelec et al, they attached SMA wire actuators to points at the inside of an airfoil. By the actuation of the SMA wires, the airfoil could be reshaped. They developed an optimization method to determine the proper placement of the SMA wire actuators within the wing. The results from the structural, thermal, and aerodynamic analysis could be put into their global optimization method to find the best configuration for the SMA wires placement.

Out-of-plane transformation of the wing

Another way of changing the aerodynamic behavior of the wing is by recasting the wing out of its original plane. Three types of such rearrangements are demonstrated in Fig 2.5 Smart materials usage for the shape morphing of wing has been extensively explored through this approach.

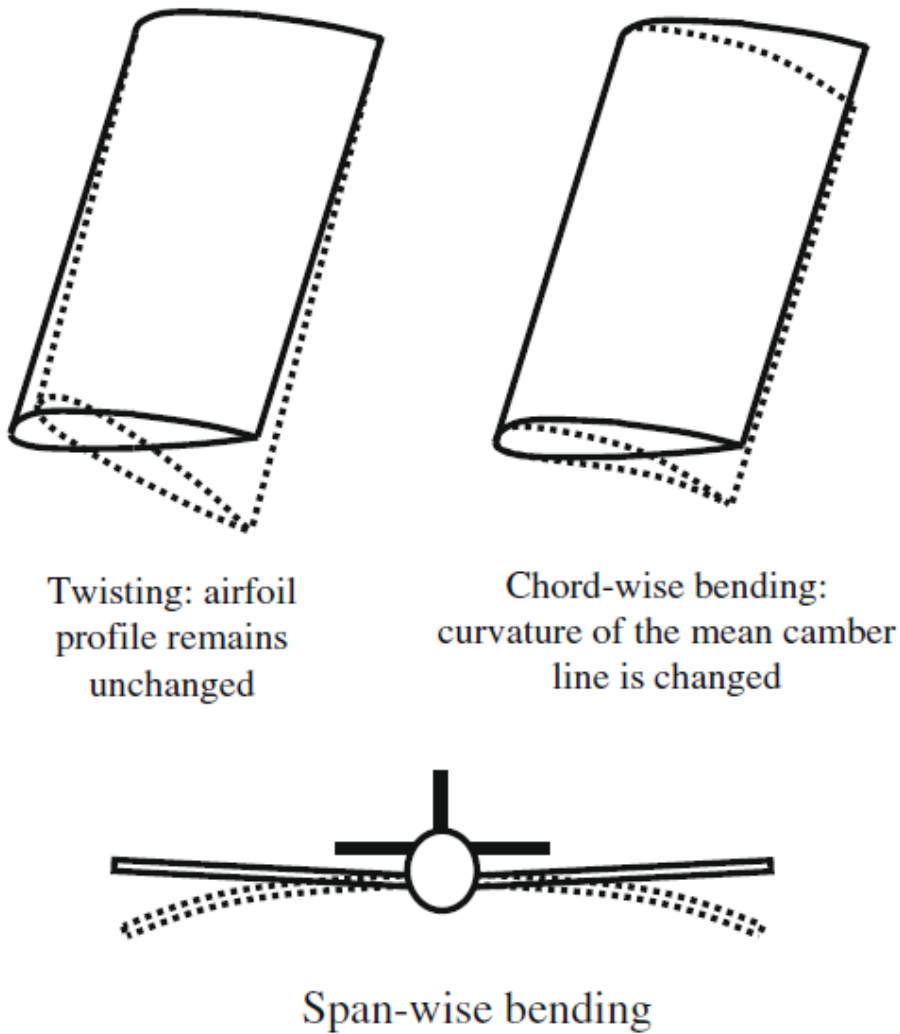


Figure 5: Out-of-plane transformation of the wing

2.3 Morphing skins

Historically, the wing skin on early aircraft was fabric but with increasing flight speeds and hence aerodynamic loads, stiffer and more robust materials were needed. The majority of aircraft today use stiffened metallic (typically aluminium alloy) panels as an outer skin, although high specific strength and stiffness fibre reinforced polymer composites in the form of glass or carbon fibre/epoxies are increasingly being employed figure(6).

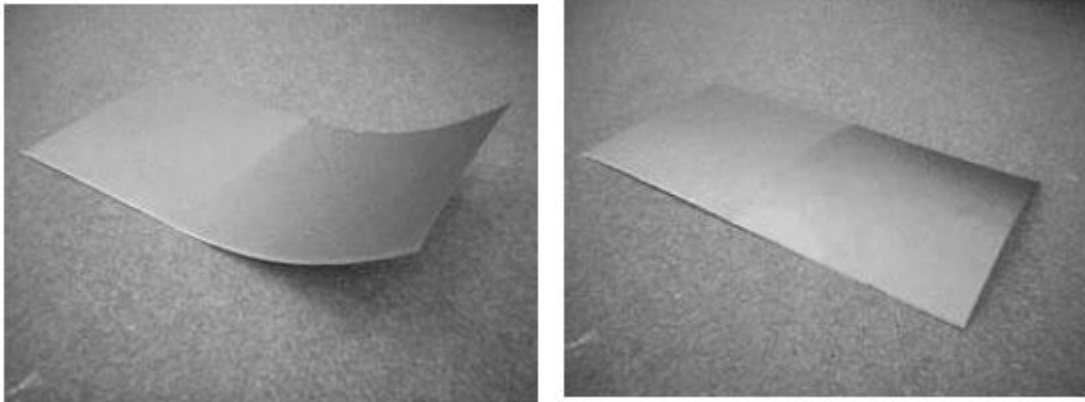


Figure 6: Composite plate

Kikuta is one of the few investigators that experimentally outline the requirements for a morphing skin of an aircraft wing [3] as follow:

- Elastic/flexible in chord wise direction to allow low force actuation.
- Stiff in span wise direction to withstand aerodynamic and inertial loads.
- Toughness.
- Abrasion and chemical resistant.
- Resistant to different weather conditions.
- High strain capability.
- High strain recovery rate.
- Environmental longevity and fatigue resistance.

2.1 Actuation for morphing technique

In order to morph the flexible skin, an actuation system must be chosen. Three actuation systems were explored to morph the wing: electromagnetic, piezoelectric, and shape memory actuators. These systems were each analyzed in terms of risk, performance, and cost. Electromagnetic actuators use solenoids to create the force to push a rod. It is this rod that is used to provide deflection for whatever purpose the actuator is being used for. The risk associated with choosing these actuators are that they are relatively large, require a fairly strong and stable material to push against since each force has an opposite and equal reaction, and they require a high power input. In terms of performance, the electromagnetic actuators produce a relatively

small stroke. However, it was determined that the cost of these actuators would be relatively moderate.

Piezoelectric actuators are ceramic actuators that convert electrical energy to mechanical energy and vice versa. The performance of piezoelectric actuators would be greater than that of electromagnetic because they have a varied stroke size. However, the main risk associated with choosing piezoelectric actuators is that they require a large amount of power to operate one actuator. The smallest actuator found, weighing 1.0 gram and having dimensions of 0.88 in. x 0.38 in. x 0.021 in., would require a minimum of 480 volts peak-to-peak to deflect the material. Piezoelectric actuators are also very high in cost.

Shape memory alloy actuation was the final system explored for the morphing process. This actuation system is an alloy material that transforms to a trained shape when heated by an electrical current and returns to its original shape when cooled below the transformation temperature. These actuators apply a force as their elongation changes during transformation. The risks associated with using this actuation system are minimal. The main risk in using the shape memory alloys is the inexperience of the group members with the use of these materials. In terms of performance, the alloys can be trained to form any desired shape, they require less power to actuate, and they can generate a large force for their small size. The cost of the material is also fairly low at approximately \$5 per foot. Table 2.1 shows the actuation system trade study assessment.

In the table, risk and performance were rated based on a scale from 1 to 10 of applicability to the project, and ability to meet the project requirements. Selection of actuators was based primarily on size, cost, and power draw. Electromagnetic actuators were found to be too large, the smallest actuators were found to be approximately 1.3 in². Piezoelectric actuators, as discussed above, draw too much power, and would therefore not be practical for use in this project.

Table 1: Actuation Design Alternatives

Options	Manufacturers	Comments	Risk	Performance	Cost
Electromagnetic	Left Hand Design Corporation	Can be made small, but not small enough Extremely small stroke Large possible power requirements	3/10	5/10	\$50
Piezo-electric		Can be made extremely small Varied stroke size Large voltage requirements, for their size extremely high cost	5/10	7/10	\$100/in ²
Shape Memory Alloys	Dynalloy, Inc	Can be trained to form any shape Achieves high temperatures Requires less power than other options Comes in many forms, so many possible design uses Force generated is large	3/10	9/10	\$5/ft

Further analysis of the trade study on these different actuation systems revealed that the most appropriate actuation system for the project involves the use of shape memory alloy actuators. The wires are small in size, relatively inexpensive, and can generate a large amount of force for their small size. Shape Memory Alloys (SMA) also provide the capability of customizing the deflections associated with force application by offering a variety of shapes and sizes used for actuation purposes. SMAs, however, do have their drawbacks. They require a very large current in order to heat them to their transformation temperature quickly. They also cause problems in designing their attachment to other structures. The resistance of the wires remains constant due to the fact that as the wire gets shorter in length, its diameter increases. This means the wire has a constant volume throughout the transformation process. So the wire cannot not be directly soldered or epoxied to a surface; since as the wire is cycled through its transformation several times it would eventually work itself loose of these attachments. However this can be easily overcome by the use of crimps on the ends of the wire and by lacing the wire onto the rib, which is discussed later in much further detail. They also can be easily over-heated or over-strained. This causes the repeatability of the wires to decrease to hundreds of times instead of

being in the thousands. In the end the problems of SMAs were deemed to be very small compared to the problems of the other types of actuators. They were not seen as to be a risk to the success of the project and minimal compared to the problems faced using other types of actuators.

2.3 Morphing Trailing edge

The following sections present some promising and relevant developments in morphing trailing edge design that's relevant to the scope of this project.

This paper represents a control of a morphing trailing edge wing by using wind tunnel tests. The work was performed under the State Key Laboratory of Mechanics and Control of Mechanical Structures, Nanjing University of Aeronautics and Astronautics, Nanjing, China.

In the previous paper, the morphing trailing edge is designed to achieve the up and down deflection under the aerodynamic load. After a detailed and accurate computational analysis to determine the SMA specifications and layout programs, a solid model is created in CATIA and the structures of the morphing wing trailing edge are produced by CNC machining. A set of DSP measurement and control system is designed to accomplish the controlling experiment of the morphing wing trailing edge. At last, via the force analysis, the trailing edge is fabricated with four sections of aluminum alloy, and the arrangement scheme of

SMA wires are determined. Experiment of precise control integral has been performed to survey the control effect. The experiment consists of deflection angle tests of the third joint and the integral structure. Primarily, the ultimate deflection angle is tested in these two experiments. Therefore, the controlling experiment of different angles could be performed within this range. The results show that the deflection error is less than 4% and response time is less than 6.7 s, the precise controlling of the morphing trailing edge is preliminary realized.

2.4 Structural design, calculation and simulation

The airfoil investigated in this paper is designed using the wing model of a certain UAV (Unmanned Aerial Vehicle). The model of airfoil (shown in Fig.7 (a)) has a chord length of 1500 mm, span length of 600 mm and maximum thickness of 263 mm. The entire airfoil model is split into a support section and a deformable trailing edge, and the major research object is the trailing edge. The length of

Support section is 900 mm and deformable trailing edge is 600 mm. Both in design and experiment, the morphing trailing edge is expected to achieve the deflection more than 8° up and down. Not only continuous deflection is essential, also the state stability at specific angles is indispensable. As the three-dimensional model shown in Fig 7 (b), the morphing structure is built in the shape of multi-joint. Every wing rib is segmented into four segments and each two adjacent segments are connected with a joint. The two wing ribs are connected and fixed by several stringers and beams. And the skin of trailing edge is fixed on the stringers as well. Therefore the stringers have the function of transferring aerodynamic load to wing ribs at the same time. As the fixed Components of SMA wires, the beams are located in the internal trailing edge. Several SMA wires are fixed at two adjacent beams to achieve the up and down deflection of every rib segment. It is obvious that three rotatable segments can reach the greater deflection angle than an integral trailing edge structure.

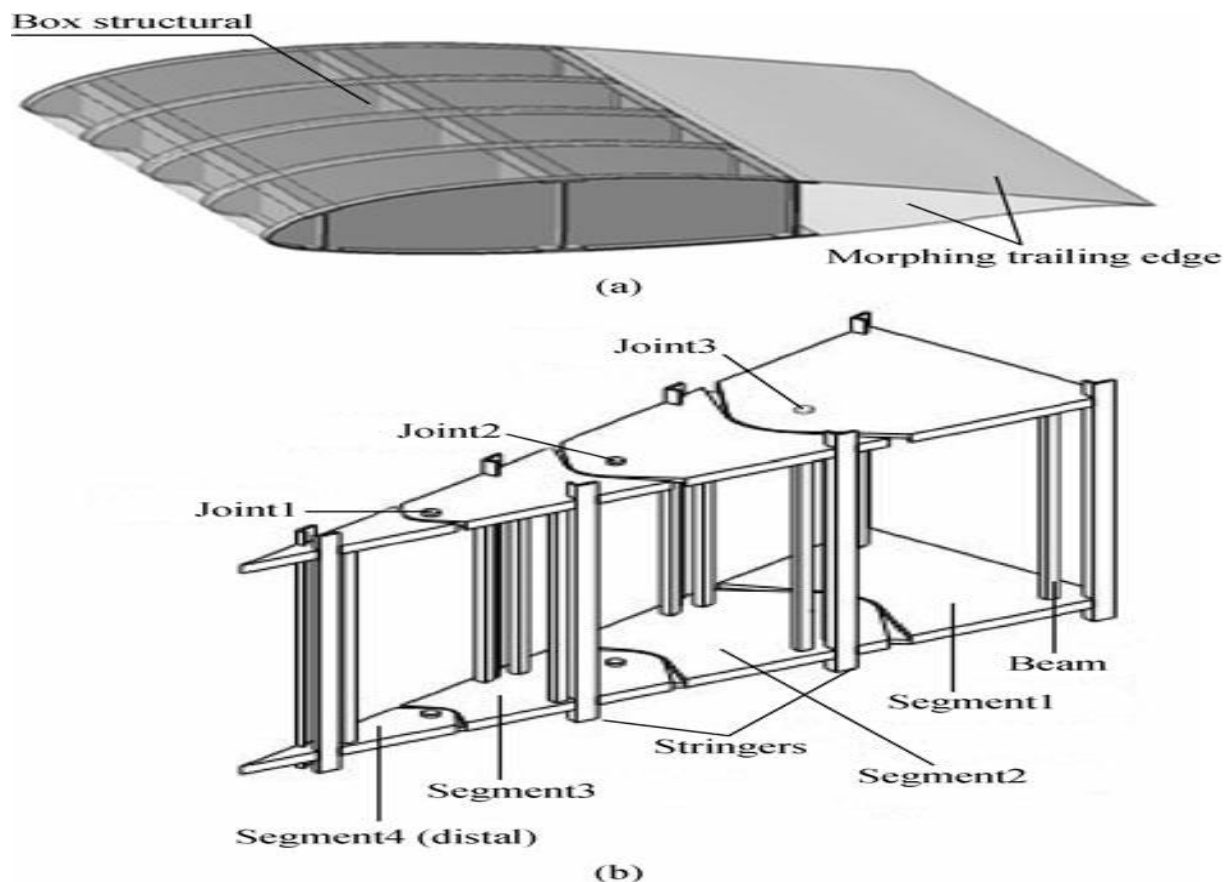


Figure 7: (a) Sketch of the airfoil model (b) 3D model morphing trailing edge structure

Based on the surface pressure coefficient data of the skin tested in wind tunnel, the aerodynamic loading imposed on the skin of trailing edge is simplified as several concentrated forces imposed on the wing ribs in the simulation and experiment. Above-mentioned wind tunnel test was conducted at the condition that Mach number is 0.4° and angle of attack is 0° . As shown in Fig 8, the simplified loads of every segment are presented. And the values of loading force are provided in Table 2, the positive number means pressure and negative number means tensile force.

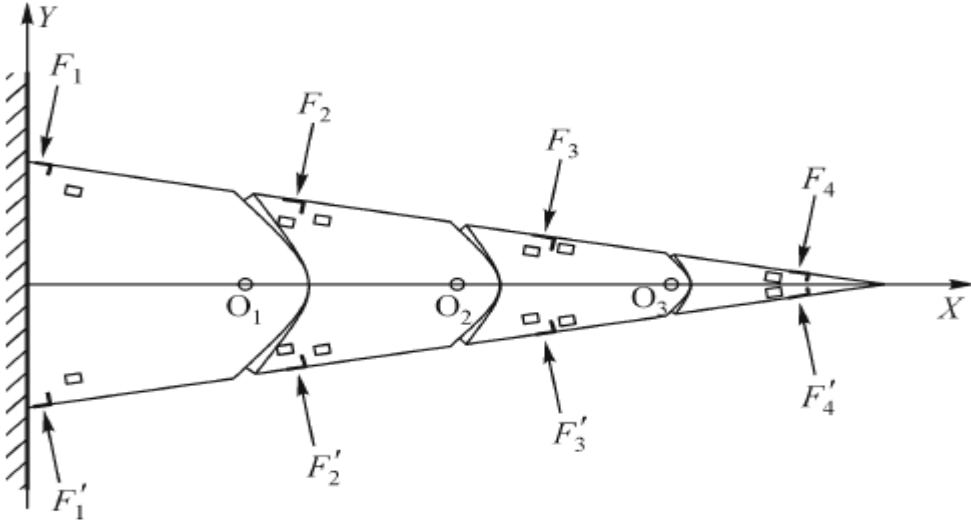


Figure 8: The sketch of concentrated forces simplified from aerodynamic loading

Table 2: Values of concentrated forces

Concentrated force	Value/N
F_1	142.98
F_2	188.48
F_3	61.54
F_4	-40.76
F_1'	33.685
F_2'	27.045
F_3'	-57.395
F_4'	-136.98

For the SMA wire actuators applied in this project, they adopt the function of constitutive model given by

$$\dot{\sigma} = E\dot{\varepsilon} + \Omega \dot{\zeta} + \theta \dot{T} \quad (1)$$

In the above equation, σ and ε present the stress and strain, E corresponds to the modulus of elasticity, Ω and θ stand for the phase change coefficient and thermoelastic coefficient, ζ and T stand for the volume percentage of martensite and temperature. After integral, one dimensional form of the constitutive model can be written as

$$\sigma - \sigma_0 = E (\varepsilon - \varepsilon_0) + \Omega (\zeta - \zeta_0) + \theta (T - T_0) \quad (2)$$

$$E (\zeta) = E_A + \zeta (E_M - E_A) \quad (3)$$

Where σ_0 , ε_0 , ζ_0 and T_0 are parameters of original state, and E_A and E_M severally stand for the modulus of elasticity in states of austenite and martensite.

The relational expression between phase change coefficient and modulus of elasticity is given by

$$\Omega (\zeta) = -\varepsilon_l E (\zeta) \quad (4)$$

Where ε_l indicates the maximum residual strain of material. When the state of SMA wire transform to austenite, the parameter ζ can be expressed as a formula with T and σ

$$\zeta = \frac{\zeta_M}{2} [\cos(a_A[T - A_s] + b_A\sigma) + 1] \quad (5)$$

And when transforming to martensite, ζ can be expressed as

$$\zeta = \frac{1-\zeta_A}{2} [\cos(a_M[T - M_f] + b_M\sigma) + \frac{1+\zeta_A}{2}] \quad (6)$$

Where the parameters a_A , a_M , b_A , and b_M are invariable of SMA material. Then they investigate the mechanical behavior of an individual rotatable (single joint) segment. Figure 9 presents a sketch of the single joint structure. SMA1 and SMA2 are pre-stretched with some pre-strain. While connecting power to SMA1, it will restore as the state before transformation due to the higher temperature, as a result, SMA2 is stretched longer with more recoverable strain. And the most ideal situation is that SMA2 possesses the most recoverable strain when SMA1 restore to the state of austenite. By computation, the maximum recoverable strain is 4.7% in the limit position. In consideration of the stress strain diagram of SMA material at lower temperature, a simplified model is presented as a spring having a stiffness of k with the addition of an initial strain value h:

$$F = kL (\sigma - \sigma_0) + h \quad (7)$$

Where $k = 1.54 \text{ N/mm}$, $h = 30\text{N}$.

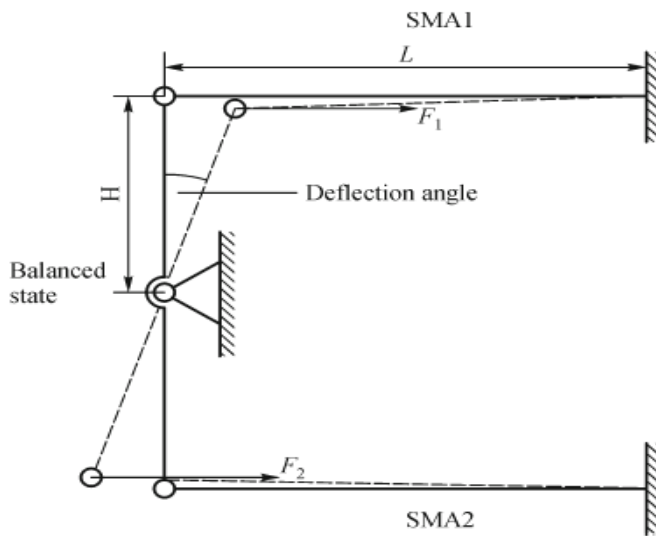
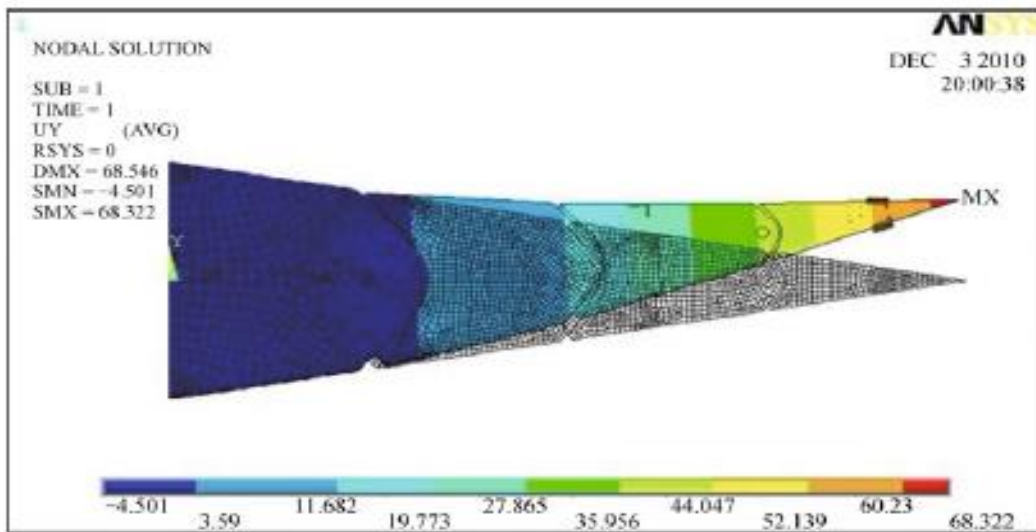
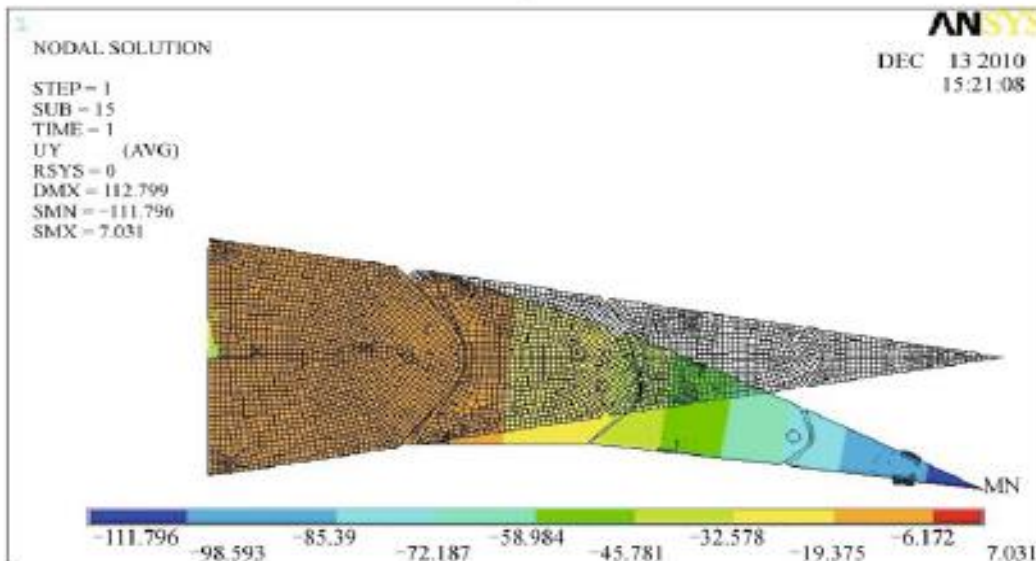


Figure 9: Sketch of SMA model arranged on a single segment

Therefore, if the four parameters a_A a_M b_A and b_M could be determined, the maximum restoring force could be calculated eventually. Due to the space limitation, the dynamic performance of SMA wires of different diameters is not listed completely. Through computing and analysis, SMA wires with the diameter of 5 mm are selected for the actuator of trailing edge structure. It is provided that maximum restoring force of single SMA wire after heated is 95.4 N and the stretching force for SMA wire in the state of martensite at normal temperature is 40.6 N. Based on the simplified aerodynamic load imposed on the morphing trailing edge structure, it is confirmed that the numbers of SMA wires arrangement on segment2 is 27, segment3 is 18 and segment4 is 10. Although experiments can provide the most accurate results, reasonable simulation can provides validation for experiment results. Through the simulation analysis by ANSYS software, the theoretical range of deflection angle is $\pm 10.337^\circ$. The simulated results are presented in Figs.10 (a) and 10 (b). It is obviously indicated that the maximum displacements of deflection upwards and downwards respectively are 68.322 and 111.796 mm which are equal to 6.496° and 10.555° converted to deflection angles.



(a)



(b)

Figure 10: (a) Simulation of deflection upward; (b) Simulation of deflection downward

2.5 Control system and methodology

In the control experiment, a measurement and control system is devised to control deflection angle of the trailing edge structure. As shown in Fig 11, the system mainly contains the trailing edge, a laser displacement sensor, a measurement and a control circuit for SMA and a DSP controller. The control process is briefly described as follows: As a start, the laser displacement sensor acquired the displacement of wingtip, and the displacement signal is input in the DSP

controller after signal conditioning. Then, control signal is output to the control circuit in the shape of PWM signal with different duty ratios (signified as q). As a final step, the PWM signal transformed by control circuit implemented the actuation for SMA wires. In the above paragraph, the control procedure is briefly demonstrated. The method adopted in the experiment is subdivision control approach uniting with PID control approach. If the error value (expressed in e) between practical deflection angle and the pre-established is greater than 0.19° , subdivision control method will be valid, else the PID control method will be. According to the PWM signal of different duty ratios generated by DSP controller, the control circuit could switch the control method between two methods. However, due to the own gravity of trailing edge, when the structure deflects downward, overshoot will be caused in case of an overlarge duty ratio. Therefore, it is obliged to actuate the SMA wires on opposite side performing more tiny deformation. As a result, the response time of the system is increased than expected.

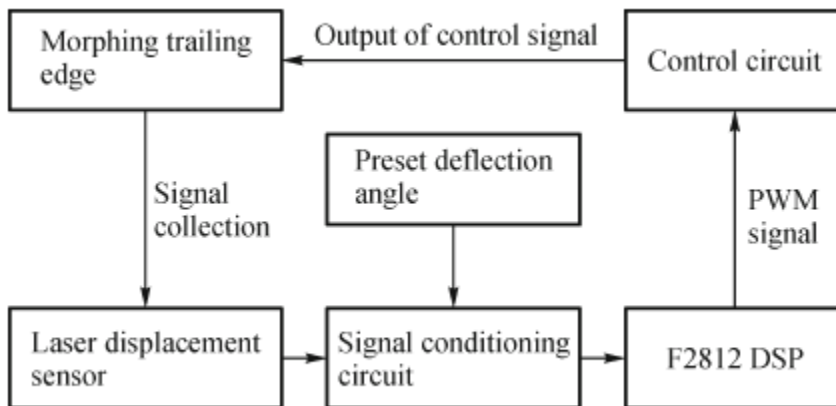


Figure 11: Sketch of measurement and control system

After many experiments, the relationship between e (error value between practical and pre-established) and q (duty ratio) in upward and downward two situations is confirmed and presented in Table (3) below.

Table 3: The relationship between e and q

	Range of e value	q value
Deflection upwards	$0.19^\circ \leq e < 0.27^\circ$	$q = 22.5\%$
	$0.27^\circ \leq e < 0.88^\circ$	$q = 45\%$
	$0.88^\circ \leq e < 2.67^\circ$	$q = 70\%$
	$e \geq 2.67$	$q = 95\%$
Deflection downwards	$0.19^\circ \leq e < 0.31^\circ$	$q = 30\%$
	$0.31^\circ \leq e < 1.15^\circ$	$q = 37.5\%$
	$1.15^\circ \leq e < 8.19^\circ$	$q = 45\%$
	$e \geq 8.19^\circ$	$q = 75\%$

When e is less than 0.19° , the control algorithm will switch to PID control method. PID algorithm can be mathematically defined as

$$U(k) = k_p e(k) + k_i \sum_{j=0}^k e(j) + k_d [e(k) - e(k-1)] \quad (8)$$

Where k is the sampling number, $u(k)$ is the data of the n th sampling, $e(k)$ is the difference value input at the n th sampling. K_P , K_I and K_D are scale factor, integral coefficient and differential coefficient of PID algorithm. Then, the three parameters mentioned above must be determined to establish the transport function between output and input of the control system. Through the process of system identification, the transport function is defined by

$$H(s) = \frac{\theta(s)}{Q(s)} = \frac{41.76s + 73.98}{s^2 - 0.06078s + 0.6468} \quad (9)$$

For the acquisition for the exact values of K_P , K_I and K_D , we accomplished the model-building and simulation in environment of MATLAB/SIMULINK software. And furthermore, the parameters are finally confirmed as: $K_P = 0.6$, $K_I = 0.3$, and $K_D = 0.01$.

2.6 Experiments and results

The whole deflection angle control experiment of the morphing trailing edge structure is made up of two major parts: (1) Control experiment of distal segment (the wingtip) separately and (2) Control experiment of integral trailing edge structure. The experimental environment and equipment is shown in Fig 12. In the experiment, the trailing edge is horizontally fixed on a foundation support which has no relative displacement with the skeleton frame. And weights are applied to simulate the simplified aerodynamic loads. The two rails arranged and fixed on the top of the skeleton frame play a role as crown blocks. Their Primary function is converting the gravity of weights to upward loading force. However, the downward loading force can be simulated with weights hanging up from the stringers located below the trailing edge.

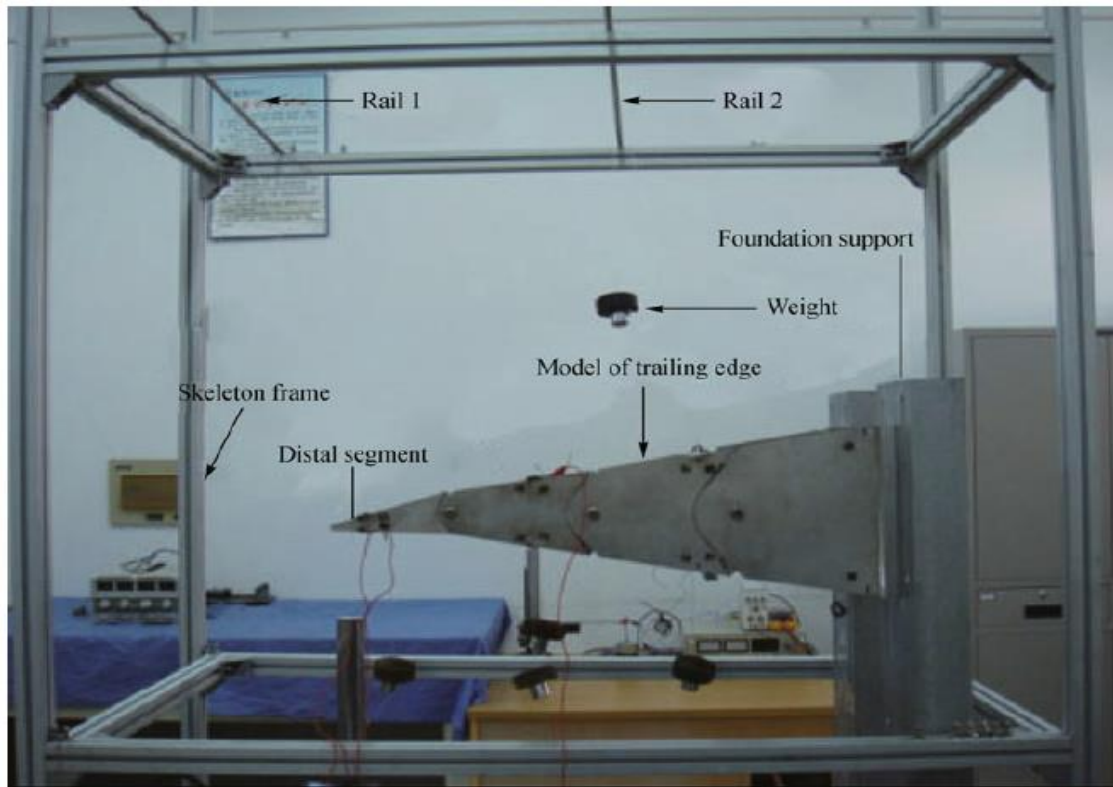


Figure 12: The experimental environment and equipment

(1) Deflection control experiment of distal segment (segment4) separately

An aim of this experiment is to obtain the Limit deflection angle of segment4. In this experiment, the segment2 and segment3 are fixed without deflection, thus only the distal segment (segment4)

could be actuated with control signal. The concrete method is setting a pre-established angle which is much greater than practical deflection angle the trailing distal segment could be performed. In this way, the distal segment would keep deflecting until reached its limit angle. So the limit angle of segment4 can be obtained. In this experiment, the pre-established upwards and downwards deflection angles are -20° and 20° . Via the experimental determination, the limit deflection angles are -9.9° upwards and 10.2° downwards (Here we make an appointment that the upwards deflection angle is expressed with negative and downwards with positive). And the displacement values of wingtip measured by laser displacement sensor are presented in Figs 13 (a) and 13 (b). Afterwards, the control effect at a certain pre-established angle is investigated. A series of angles in Table 2.3 are given to the control system, including four negative angles and four positive ones. In the end, the result data items are shown in Table 4 as well. The control result of deflection downward with 1° and PWM control signal are shown in Fig14 as a typical case. Response times of SMA actuators and errors between the practical deflection angles and the target angles of eight different angles are shown in Table 2.3. From Table 2.3, we found that error values between practical angles and ideals are less than 5% completely, and response time values are less than 5.5 s overall. In view of above mentioned, the control system should be regarded as a coincidence with expected. As mentioned earlier in this paper, the response times in the case of downwards deflection are generally some longer than upwards deflection. Then we investigated the reasons which caused the above phenomenon in detail. One main factor is the own gravity of the distal segment which makes itself having a trend to deflect downwards, and another factor is the heat-up time of SMA wires which impacts the response time.

Table 4: The response times and the errors between the practical deflection angles and the target angles

	Target deflection angle/(°)	Practical deflection angle/(°)	Relative error/%	Response time/s
Deflection upwards	-1	-0.97	3.0	2.70
	-3	-2.97	1.0	2.70
	-5	-4.95	1.0	2.36
	-7	-6.97	0.4	4.67
Deflection downwards	1	1.04	4.0	5.38
	3	3.03	1.0	3.08
	5	5.05	1.0	3.47
	7	7.04	0.6	4.80

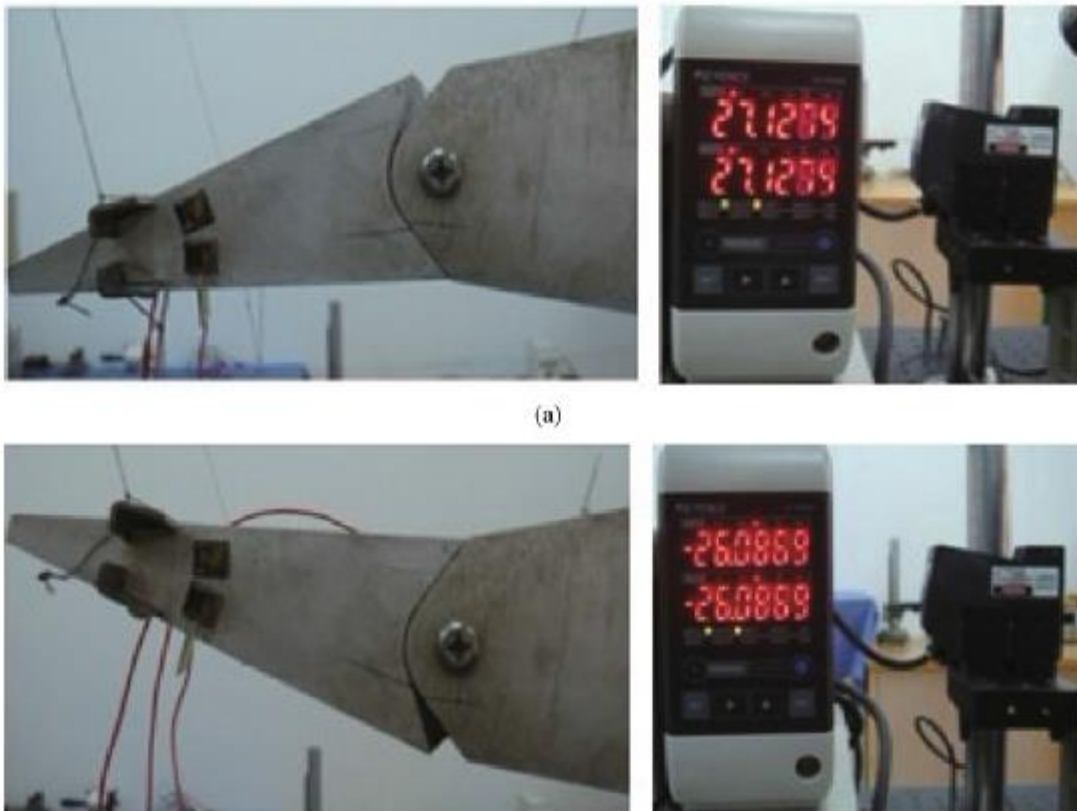


Figure 13: (a) The wingtip displacement of deflection downwards; (b) The wingtip displacement of deflection upwards

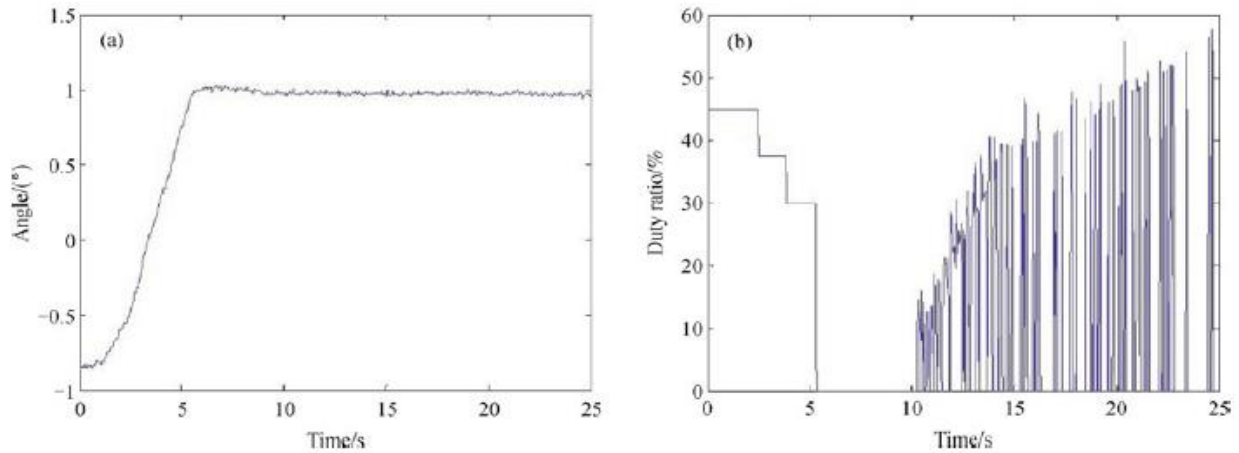


Figure 14: (a) The control effect at 1°; (b) PWM signal pattern in the control procedure

(2) Deflection control experiment of the trailing edge structure entirety

The significance of this experiment is to test and verify the continuity of deflection and the bearing reliability of the structure. Analogously as the previous experiment, the limit deflection angle is necessary to be acquired as the first step. And the pre-established deflection angles are same as previous. By the experiment the limit deflection angles are determined as -8.5° upwards and 10.4° downwards. In theory, integral deflection angle is equal to the sum of three deflection angles of segment1, segment2 and segment3. However, the actual deflection angle of each rotatable segment could not reach the limiting angle subject to the elasticity of SMA wires.

In Fig 15 the limit deflection angles testing experiment is presented. Next, the control effect at a specific angle of the whole morphing trailing edge will be investigated. Here the targeted deflection angles are set as -3° upwards and 3° downwards. As the results shown in Fig 16, the response time is 2.7 s and practical deflection angle is -2.96° , the relative error is 1.3%. In the case of deflection downwards of 3° , the response time and relative error are respectively 6.7 s and 0.3%. Because of the influence of gravity and the inertia of loads imposed on the structure, the response time of deflection downwards is obviously larger than the one in the case upwards.



Figure 16: Sketch of integral deflection

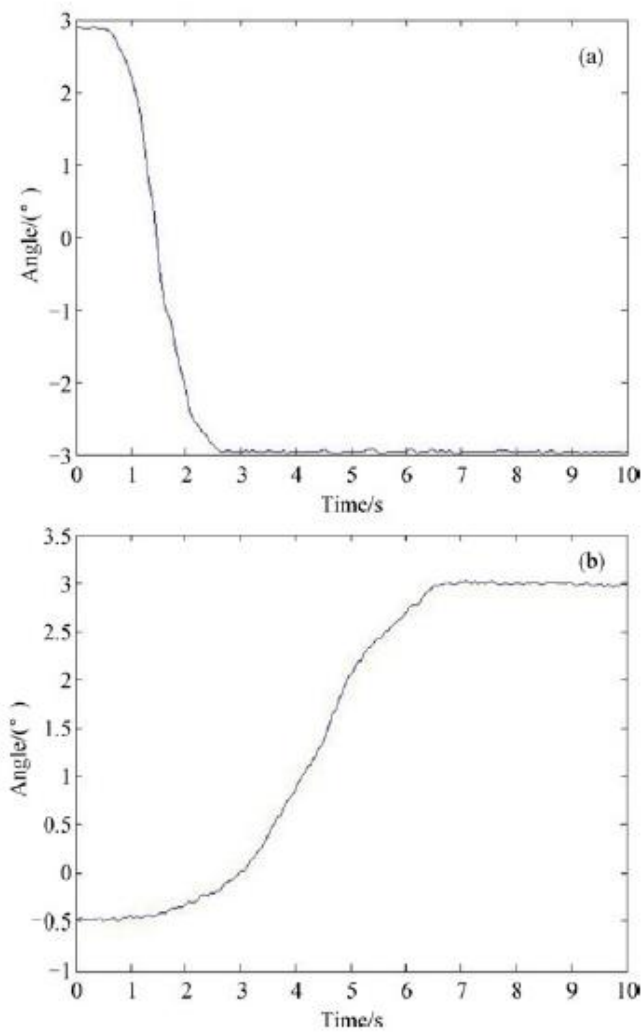


**Figure 17: (a) The control effect at -3° of integral deflection upwards
(b) The control effect at 3 degrees of integral deflection downwards**

Chapter 3: Model Descriptions

3.1 Morphing Trailing Edge Wing Model

Model fabricated by Ermira Junita Abdullah at university of RMIT August 2011[9] was used Clark Y as the airfoil due to its excellent performance at low speeds fig 18, Clark Y airfoil was chosen with a chord of 247 mm and a span of 285 mm. ABS was selected as the skin material as it can produce the biggest trailing edge deflection when actuated, while still retaining its shape, the skin thickness was chosen such that the airfoil is able to morph while minimizing the occurrence of buckling.

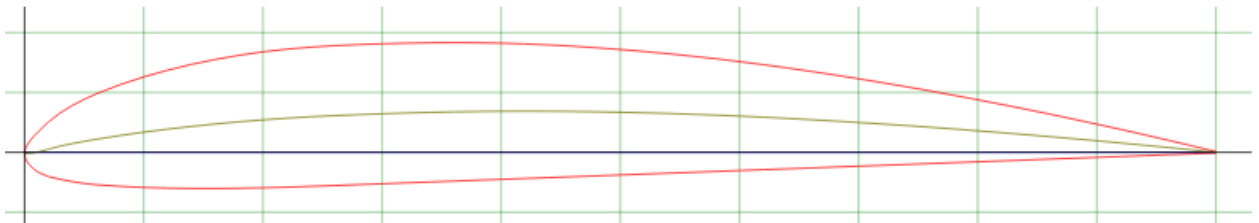


Figure 18: Clark Y airfoil

Due to space constraint in the trailing edge, it was decided that the SMA actuator will be placed only near the leading edge. The actuator was attached to two points near the leading edge of the airfoil, placement of the actuator is critical in obtaining the desired change of the airfoil camber. A different combination of applied forces by the SMA actuator was analysed. The actuators were attached to two points on the upper side of the airfoil and two points on the lower side of the airfoil. The coordinates of the points are (0.17, 0.08), (0.35, -0.03), (0.8, 0.4) and (0.6, -0.2).fig 19

The SMA wires used in this model were FLEXINOL® wires which were pre-crimped with ring crimps produced by Dynalloy Inc, see table

In order to increase the pull force of the SMA actuators while still preserving the contraction properties, they were constructed in a bundle which consisted of a multitude of wires in parallel attached to a bracket by crimps at the both ends of the actuator, the need to produce large force from the actuator is achieved by bundling the wires without sacrificing actuation time. It might be regarded that the best circuit design for the bundle is a parallel arrangement

of the wires, but this will result in impractical power supply requirements, a bundle length of 35 mm

A single 0.3048mm diameter wire has a pull force of 1250g, so in theory, 4 wires of 0.3048 mm connected mechanically in parallel has a total pull force of at least 40N. Since the span of the wing is 285 mm, fourteen SMA wire bundles were needed so in total, 56 SMA wires were used. The wire bundles were connected mechanically in parallel but they were connected electrically in series.fig 20

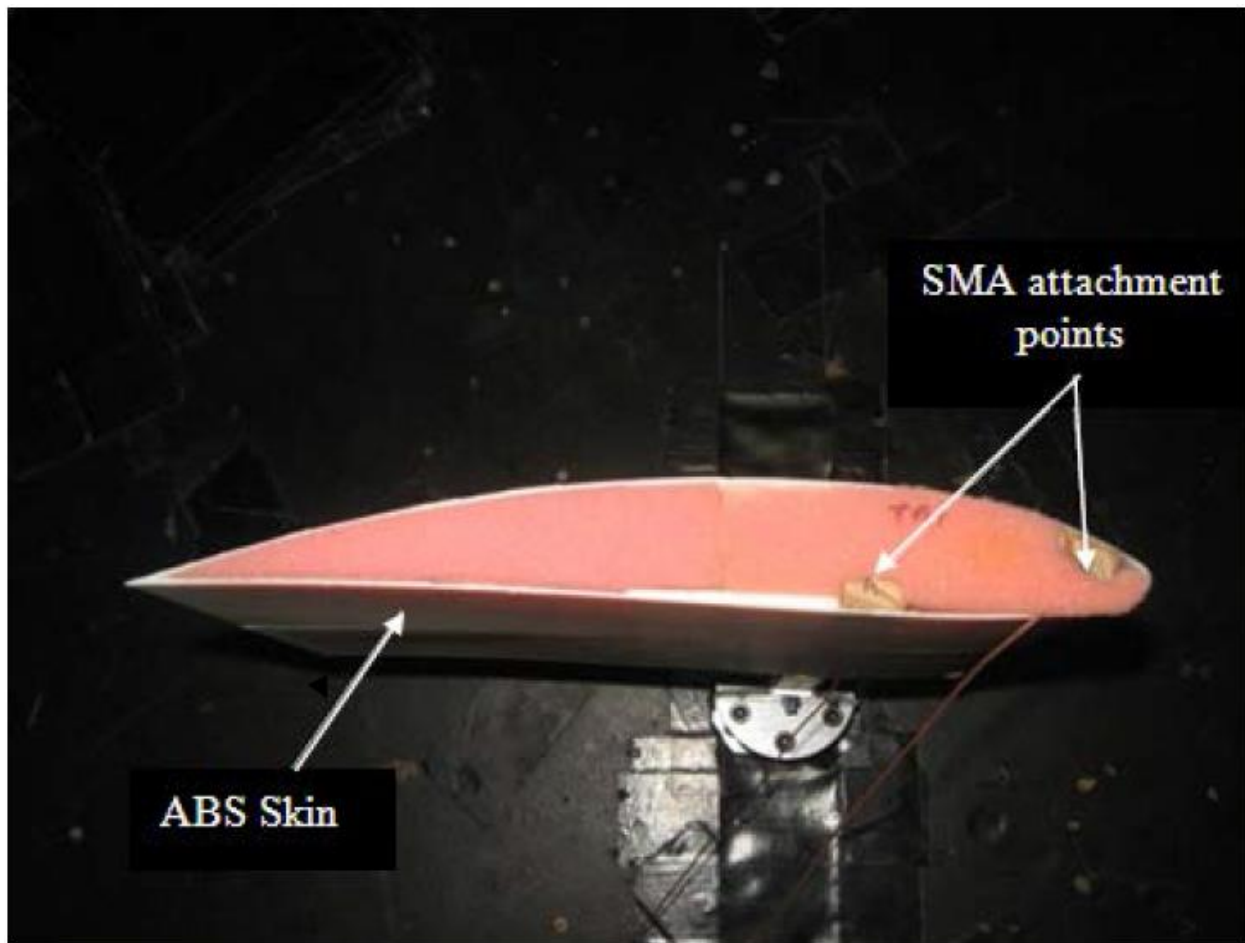


Figure 19: Side view of the experimental wing model

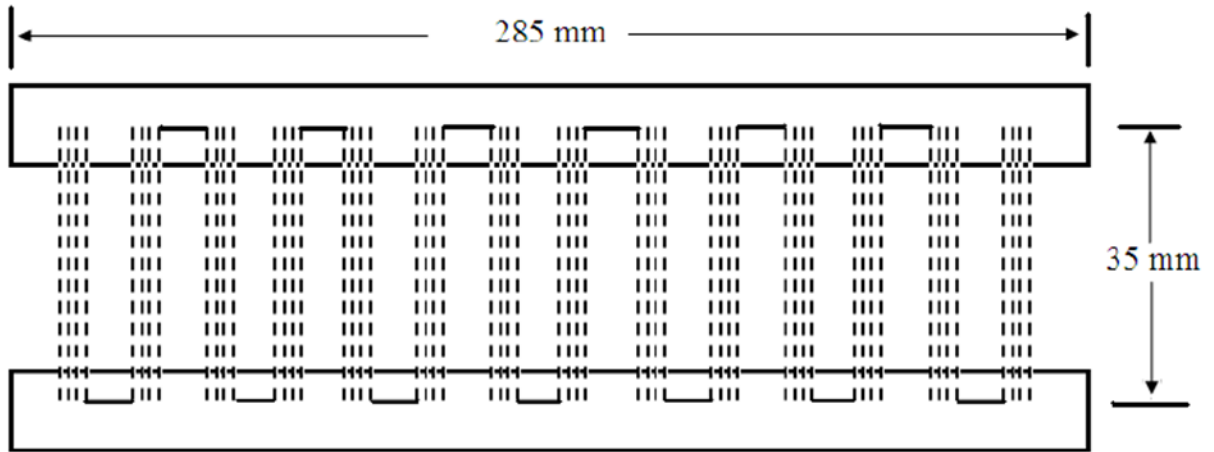


Figure 20: Schematic diagram of the SMA actuators layout (top view)

The SMA actuators were powered by current supplied by the Manson NP-9615 regulated dc power supply with a range of 0-20 V or 0-10 A

Table 5: Specifications of nickel titanium (SMA) wire FLEXINOL® wires

Parameters	Value
Mass per unit length (m in $kg.m^{-1}$)	$4.54e^{-4}$
Specific heat capacity (c_p in $J.kg^{-1}.K^{-1}$)	320
Resistance per unit length (R in $\Omega.m^{-1}$)	12.2
Thermal expansion (θ_f in $N.m^{-2}.K^{-1}$)	$-11e^{-6}$
SMA initial strain (ε_i)	0.03090
Heat convection coefficient (h_0 in $J.m^{-2}.s^{-1}.K^{-1}$)	28.552
Heat convection coefficient (h_2 in $J.m^{-2}.s^{-1}.K^{-1}$)	$4.060e^{-4}$
Diameter of wire (in m)	$305e^{-6}$
Length of wire (in m)	0.035
Ambient temperature (T_a in $^{\circ}C$)	20
Martensite to austenite transformation temperature (A_f in $^{\circ}C$)	70
Austenite to martensite transformation temperature (M_f in $^{\circ}C$)	55
Spread of temperature around A_f (σ_a in $^{\circ}C$)	6
Spread of temperature around M_f (σ_a in $^{\circ}C$)	4.5

3.2 Shape memory alloys Actuator

Shape memory materials have been the focus of many researchers only recently although the one-way shape memory effect was first observed by Chang and Read in 1951 for a gold-cadmium alloy. In 1963 Buehler et al developed the SME of nickel titanium alloy, commercialized under the trade name Nitinol an acronym for Nickel Titanium Naval Ordnance Laboratories.

The one-way SME for an alloy is defined as a change in shape of the material due to a change in temperature which is called a thermally induced shape-memory effect. The shape memory alloy (SMA) is cooled from its austenite phase (possible temperature range 52°C to 77°C) to its twinned martensite phase (possible temperature range -20°C to 35°C), note that there is no change in shape during this phase transformation process. In this latter phase it has low stiffness and can be deformed easily. Hence when a load is applied the SMA can be changed in shape to a deformed temporary martensite phase. When heated above its austenite finish temperature it will return to its original shape in the austenite phase (Fig 21)

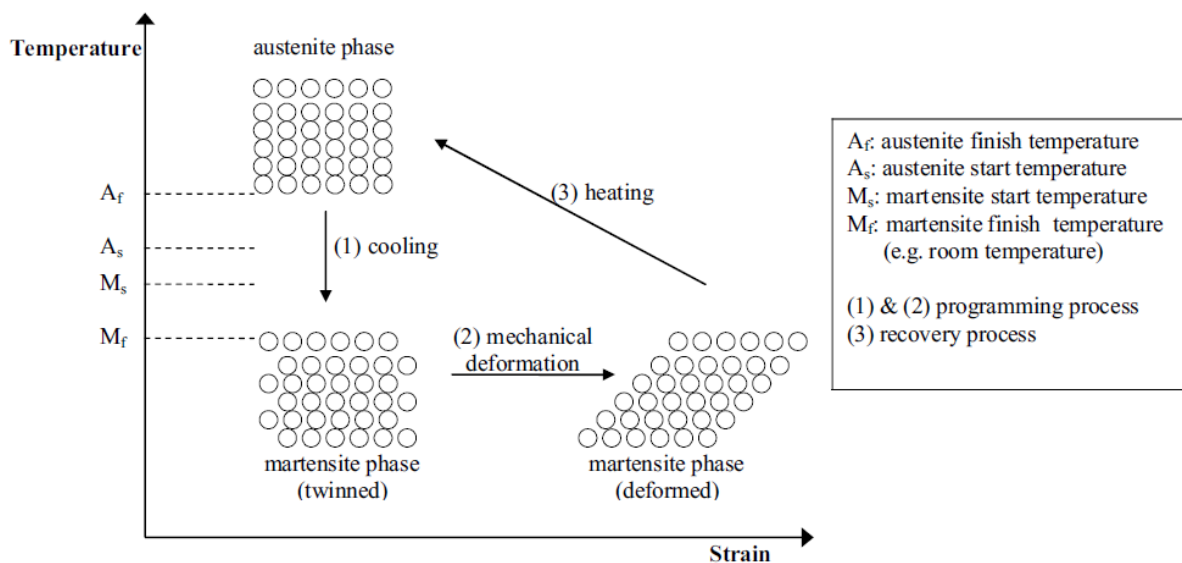


Figure 21: Heating and Cooling of SMA

Typically a recovery of the memorized shape for deformations of up to 8% plastic strain and a two- to fourfold increase in Young's Modulus can be observed. This is called one-way SME. The shape that a SMA memorizes can be assigned or reassigned through an annealing process (heating above 500°C). More recent research has shown that the two-way SME can be achieved after certain thermal training which involves repeating the one-way SME cycle several times. This means that the SMA can switch between two configurations when heated and cooled. There is a third effect that SMAs encounter which is called pseudoelasticity, Pseudoelasticity or superelasticity is the effect of shifting of the transformation temperatures and, in some cases, to partial or even total formation of martensite of SMAs in the austenite phase when subjected to stress at constant high temperatures.

This implies that, in general, transformation temperatures of a given alloy increase with increasing applied stress. A final general point to make about SMAs is the presence of temperature hysteresis which means that the change from martensite to austenite during heating occurs at a higher temperature than the change from austenite to martensite during cooling.

3.3 ABS Skin

Chemical formula $(C_8H_8)_x \cdot (C_4H_6)_y \cdot (C_3H_3N)_z$ is a common thermoplastic polymer. Its glass transition temperature is approximately 105 °C (221 °F), ABS is amorphous and therefore has no true melting point.

ABS is a terpolymer made by polymerizing styrene and acrylonitrile in the presence of polybutadiene. The proportions can vary from 15 to 35% acrylonitrile, 5 to 30% butadiene and 40 to 60% styrene. The result is a long chain of polybutadiene criss crossed with shorter chains of poly(styrene-co-acrylonitrile). The nitrile groups from neighboring chains, being polar, attract each other and bind the chains together, making ABS stronger than pure polystyrene. The styrene gives the plastic a shiny, impervious surface. The polybutadiene, a rubbery substance, provides toughness even at low temperatures. For the majority of applications, ABS can be used between -20 and 80 °C (-4 and 176 °F) as its mechanical properties vary with temperature. The properties are created by

rubber toughening, where fine particles of elastomer are distributed throughout the rigid matrix.

The most important mechanical properties of ABS are impact resistance and toughness. A variety of modifications can be made to improve impact resistance, toughness, and heat resistance. The impact resistance can be amplified by increasing the proportions of polybutadiene in relation to styrene and also acrylonitrile, although this causes changes in other properties. Impact resistance does not fall off rapidly at lower temperatures. Stability under load is excellent with limited loads. Thus, by changing the proportions of its components, ABS can be prepared in different grades. Two major categories could be ABS for extrusion and ABS for injection moulding, then high and medium impact resistance. Generally ABS would have useful characteristics within a temperature range from -20 to 80 °C (-4 to 176 °F).[4]

The final properties will be influenced to some extent by the conditions under which the material is processed to the final product. For example, molding at a high temperature improves the gloss and heat resistance of the product whereas the highest impact resistance and strength are obtained by molding at low temperature. Fibers (usually glass fibers) and additives can be mixed in the resin pellets to make the final product strong and raise the operating range to as high as 80 °C (176 °F). Pigments can also be added, as the raw material original color is translucent ivory to white. The aging characteristics of the polymers are largely influenced by the polybutadiene content, and it is normal to include antioxidants in the composition. Other factors include exposure to ultraviolet radiation, for which additives are also available to protect against.

ABS polymers are resistant to aqueous acids, alkalis, concentrated hydrochloric and phosphoric acids, alcohols and animal, vegetable and mineral oils, but they are swollen by glacial acetic acid, carbon tetrachloride and aromatic hydrocarbons and are attacked by concentrated sulfuric and nitric acids. They are soluble in esters, ketones, ethylene dichloride and acetone.[2]

Even though ABS plastics are used largely for mechanical purposes, they also have electrical properties that are fairly constant over a wide range of frequencies. These

properties are little affected by temperature and atmospheric humidity in the acceptable operating range of temperatures.

ABS is flammable when it is exposed to high temperatures, such as a wood fire. It will melt then boil, at which point the vapors burst into intense, hot flames. Since pure ABS contains no halogens, its combustion does not typically produce any persistent organic pollutants, and the most toxic products of its combustion or pyrolysis are carbon monoxide and hydrogen cyanide. ABS is also damaged by sunlight. This caused one of the most widespread and expensive automobile recalls in US history due to the degradation of the seatbelt release buttons.

3.4 Test Result of wind tunnel

It is necessary to conduct the control experiment in environments which are close to the real application, the objective of the wind tunnel tests was to create an environment of varying velocity and angle of attack, to study the robustness of the control system for a morphing trailing edge wing in flying conditions.

Experimental carried by the RMIT Aerospace group were at Reynolds number 1.0×10^5 and 0° angle of attack fig 3.5, and it shows the following results see table 3.2

Wing mounted on a strut in the wind tunnel [9]

Table 6: trailing edge deflection of the wing panel ith ABS skin

1st SMA actuator	2nd SMA actuator	Trailing edge deflection
10 N	10 N	9.13 mm
10 N	20 N	18.11 mm
10 N	50 N	45.03 mm
20 N	10 N	9.29 mm
20 N	20 N	18.37 mm
20 N	50 N	45.20 mm
50 N	10 N	9.79 mm
50 N	20 N	18.77 mm

Chapter 4: Control System For A Morphing Trailing Edge

4.1 Control Theory

Is an interdisciplinary branch of engineering and mathematics that deals with the behaviour of dynamical with inputs, and how their behaviour is modified by feedback. the usual objective of control theory is to control a system, often called the plant, so its output follows a desired control signal, called the reference, which may be a fixed or changing value. To do this a controller is designed, which monitors the output and compares it with the reference. The difference between actual and desired output, called the error signal, is applied as feedback to the input of the system, to bring the actual output closer to the reference. Some topics studied in control theory are stability (whether the output will converge to the reference value or oscillate about it), controllability and observability.[6]

Classical Control Theory

To overcome the limitations of the open-loop controller, control theory introduces feedback. Closed-loop controller uses feedback to control states or outputs of a dynamical system. Its name comes from the information path in the system: process inputs (e.g., voltage applied to an electric motor) have an effect on the process outputs (e.g., speed or torque of the motor), which is measured with sensors and processed by the controller; the result (the control signal) is "fed back" as input to the process, closing the loop.

Closed-loop controllers have the following advantages over open-loop controllers:

1. Disturbance rejection (such as hills in the cruise control example above).
2. Guaranteed performance even with model uncertainties, when the model structure does not match perfectly the real process and the model parameters are not exact.
3. Unstable processes can be stabilized.
4. Reduced sensitivity to parameter variations.
5. Improved reference tracking performance.

In some systems, closed-loop and open-loop control are used simultaneously. In such systems, the open-loop control is termed feed forward and serves to further improve reference tracking performance. Common closed-loop controller architecture is the PID controller.

Modern Control Theory

In contrast to the frequency domain analysis of the classical control theory, modern control theory utilizes the time-domain state space representation, a mathematical model of a physical system as a set of input, output and state variables related by first-order differential equations. To abstract from the number of inputs, outputs and states, the variables are expressed as vectors and the differential and algebraic equations are written in matrix form (the latter only being possible when the dynamical system is linear).[3]

The state space representation (also known as the "time-domain approach") provides a convenient and compact way to model and analyse systems with multiple inputs and outputs. With inputs and outputs, we would otherwise have to write down Laplace transforms to encode all the information about a system.

Unlike the frequency domain approach, the use of the state-space representation is not limited to systems with linear components and zero initial conditions. "State space" refers to the space whose axes are the state variables. The state of the system can be represented as a vector within that space.

Optimal Control Theory

Optimal control deals with the problem of finding a control law for a given system such that a certain optimality criterion is achieved. A control problem includes a functional that is a function of state and control variables. An optimal control is a set of differential equations describing the paths of the control variables that minimize the cost functional. The optimal control can be derived using Pontryagin's maximum principle (a necessary condition also known as Pontryagin's minimum principle or simply Pontryagin's Principle), or by solving the Hamilton–Jacobi–Bellman equation (a sufficient condition).

Control Design Requirements

1. Regulation: keep controlled variable near a constant target value (e.g. process control: pressure, concentration etc.).
2. Tracking: keep controlled variable near a time-varying target value (e.g. antenna positioning, robotic manipulator point-to point manoeuvre, motor speed/position control).

3. Stability, roughly means bounded output for bounded input,
4. Accuracy means minimum steady state error.
5. Satisfactory transient behaviour means minimum or zero overshoot, fast response (less rise and settling times).
6. Robustness means less sensitivity to real operating conditions abrupt changes.

4.2 Types of PID Controllers

Most control systems in the past were implemented using mechanical systems or solid state electronics. Pneumatics was often utilized to transmit information and control using pressure. However, most modern control systems in industrial settings now rely on computers for the controller. Obviously it is much easier to implement complex control algorithms on a computer than using a mechanical system.

1. Proportional Controller

We cannot use types of controllers at anywhere, with each type controller; there are certain conditions that must be fulfilled. With proportional controllers there are two conditions and these are written below:

- Deviation should not be large, it means there should be less deviation between the input and output.
- Deviation should not be sudden.

Now we are in a condition to discuss proportional controllers, as the name suggests in a proportional controller the output (also called the actuating signal) is directly proportional to the error signal. Now let us analyse proportional controller mathematically. As we know in proportional controller output is directly proportional to error signal, writing this mathematically we have,

$$A(t) \propto e(t) \dots \dots \dots (4.1)$$

Removing the sign of proportionality we have,

$$A(t) = Kp \times e(t) \dots \dots \dots (4.2)$$

Where:

Kp is proportional constant also known as controller gain. It is recommended that Kp should be kept greater than unity. If the value of Kp is greater than unity, then it will amplify the error signal and thus the amplified error signal can be detected easily. Proportional controller helps in reducing the steady state error, thus makes the system more stable. Slow response of the over damped system can be made faster with the help of these controllers. Now there are some serious disadvantages of these controllers and these are written as follows:

- Due to presence of these controllers there are some offsets in the system.
- Proportional controllers also increase the maximum overshoot of the system.

2. Integral Controller

As the name suggests in integral controllers the output (also called the actuating signal) is directly proportional to the integral of the error signal. Now let us analyze integral controller mathematically. As we know in an integral controller output is directly proportional to the integration of the error signal, writing this mathematically we have,

$$A(t) \propto \int_0^t e(t)dt \dots\dots\dots (4.3)$$

Removing the sign of proportionality we have,

$$A(t) = Ki \times \int_0^t e(t)dt \dots\dots\dots (4.4)$$

Where:

Ki is integral constant also known as controller gain. Integral controller is also known as reset controller. Due to their unique ability they can return the controlled variable back to the exact set point following a disturbance that's why these are known as reset controllers. Integral Controller has advantages that it tends to make the system unstable because it responds slowly towards the produced error. [5]

3. Derivative Controller

We never use derivative controllers alone. It should be used in combinations with other modes of controllers because of its few disadvantages which are written below:

- It never improves the steady state error.
- It produces saturation effects and also amplifies the noise signals produced in the system.

Now, as the name suggests in a derivative controller the output (also called the actuating signal) is directly proportional to the derivative of the error signal. Now let us analyze derivative controller mathematically. As we know in a derivative controller output is directly proportional to the derivative of the error signal, writing this mathematically we have,

$$A(t) \propto \frac{de(t)}{dt} \dots\dots\dots (4.5)$$

Removing the sign of proportionality we have,

$$A(t) = Kd \times \frac{de(t)}{dt} \dots\dots\dots (4.6)$$

Where:

Kd is proportional constant also known as controller gain. Derivative controller is also known as rate controller. The major advantage of derivative controller is that it improves the transient response of the system.

4. PID Controller

The PID controller calculation (algorithm) involves three separate parameters; the Proportional, the Integral and Derivative values. The Proportional value determines the reaction to the current error, the Integral determines the reaction based on the sum of recent errors and the Derivative determines the reaction to the rate at which the error has been changing. The weighted sum of these three actions is used to adjust the process via a control element such as the position of a control valve or the power supply of a heating element.

Some applications may require using only one or two modes to provide the appropriate system control. This is achieved by setting the gain of undesired control outputs to zero. A PID controller will be called a PI, PD, P or I controller in the absence of the respective control actions. PI controllers are particularly common, since derivative action is very sensitive to measurement noise, and the absence of an integral value may prevent the system from reaching its target value due to the control action.

5. Proportional and Integral Controller

As the name suggests it is a combination of proportional and an integral controller the output (also called the actuating signal) is equal to the summation of proportional and integral of the error signal. Now let us analyse proportional and integral controller mathematically. As we know in a proportional and integral controller output is directly proportional to the summation of proportional of error and integration of the error signal, writing this mathematically we have,

$$A(t) \propto \int_0^t e(t) + A(t) \propto e(t) \dots \dots \dots (4.7)$$

Removing the sign of proportionality we have,

$$A(t) = Ki \int_0^t e(t)dt + Kp e(t) \dots \dots \dots (4.8)$$

Where:

Ki and Kp are proportional constant and integral constant respectively.

Advantages and disadvantages are the combinations of the advantages and disadvantages of proportional and integral controllers.

6. Proportional and Derivative Controller

As the name suggests it is a combination of proportional and a derivative controller the output (also called the actuating signal) is equals to the summation of proportional and derivative of the error signal. Now let us analyze proportional and derivative controller mathematically. As we know in a proportional and derivative controller output is directly proportional to summation of proportional of error and differentiation of the error signal, writing this mathematically we have,

$$A(t) \propto \frac{de(t)}{dt} + A(t) \propto e(t) \dots \dots \dots (4.9)$$

Removing the sign of proportionality we have,

$$A(t) = Kd \frac{de(t)}{dt} + Kpe(t) \dots \dots \dots (4.10)$$

Where:

Kd and Kp are proportional constant and derivative constant respectively.

Table 7: Effects of coefficients

CL RESPONSE	RISE TIME	OVERSHOOT	SETTLING TIME	S-S ERROR
K_p	Decrease	Increase	Small Change	Decrease
K_i	Decrease	Increase	Increase	Eliminate
K_d	Small Change	Decrease	Decrease	Small Change

4.3 Response analyze of the PID controller

Advantages and disadvantages are the combinations of advantages and disadvantages of proportional and derivative controllers. By "tuning" the three constants in the PID controller algorithm the PID can provide control action designed for specific process requirements. The response of the controller can be described in terms of the responsiveness of the controller to an error, the degree to which the controller overshoots the set point and the degree of system oscillation. Note that the use of the PID algorithm for control does not guarantee optimal control of the system or system stability. See table 4.1 and 4.2

Effects of coefficients

Effects of each of controller K_p, K_d, and K_i on a closed-loop system

The transient response of a practical control system often exhibits damped oscillations before reaching steady state. In specifying the transient-response characteristics of a control system to a unit-step input, it is common to specify the following:

Delay time (t_d): The delay time is the time required for the response to reach half the final value the very first time.

Table 8: Effects of each of controller K_p, K_d, and K_i on a closed-loop system

Parameter	Speed of response	Stability	Accuracy
increasing K	increases	deteriorate	improves
increasing K _i	decreases	deteriorate	improves
increasing K _d	increases	improves	no impact

Rise time (t_r): The rise time is the time required for the response to rise from (10% to 90%), (5% to 95%) or (0% to 100%) of its final value. For under damped second order systems, the (0% to 100%) rise time is normally used. For over damped systems, the (10% to 90%) rise time is commonly used.

Peak time (t_p): The peak time is the time required for the response to reach the first peak of the overshoot.

Maximum overshoot (per cent): The maximum overshoot is the maximum peak value of the response curve measured from unity.

Settling time (t_s): The settling time is the time required for the response curve to reach and stay within a range about the final value of size specified by absolute percentage of the final value (usually 2% or 5%).

These specifications are shown graphically in figure4.1

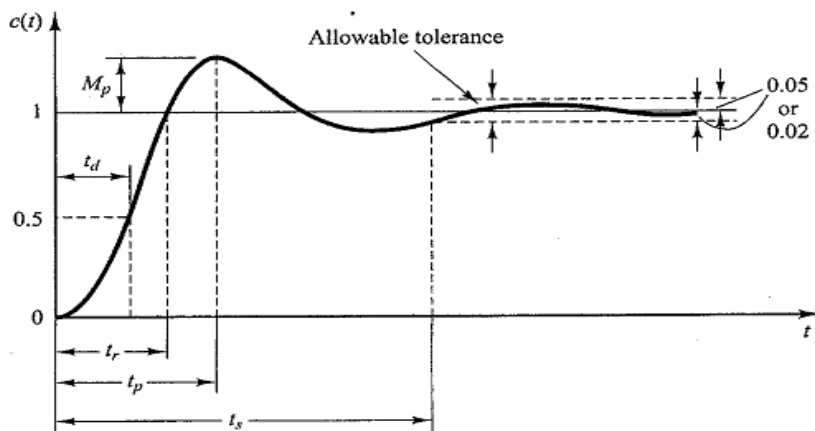


Figure 22: Transient and Steady-State Response Analyses

4.4 Mathematical model of the SMA actuator

The model describing the SMA wire actuators behaviour is readily available. The important temperature parameters that describe the SMA model are martensite finish temperature (M_f), martensite start temperature (M_s), austenite start temperature (A_s) and austenite finish temperature (A_f). The SMA model being considered here is characterized by $A_s > M_s$. Liang has derived a relation between martensite fraction and temperature ($\zeta - T$) using a cosine function. The

two equations describing the martensite fraction during the transformation under free stress condition from M→A and M←A are given as

$$\zeta = \frac{1}{2} [\cos(a_A [T - A_s]) + 1] \dots \dots \dots (4.11)$$

$$\zeta = \frac{1}{2} [\cos(a_M [T - M_f]) + 1] \dots \dots \dots (4.12)$$

where the two material constants a_A and a_M are determined from

$$a_A = \pi / (A_f - A_s)$$

$$a_M = \pi / (M_s - M_f)$$

If the M→A transformation starts from a state that has mixed austenite and martensite phases, denoted by (ζ_M, T_M) , it is assumed that during the heating process, there will be no new austenite phase until the temperature is higher than A_s . The transformation for temperatures above A_s is described by

$$\zeta = \frac{\zeta_M}{2} [\cos(a_A [T - A_s]) + 1] \dots \dots \dots (4.13)$$

If M←A transformation starts from (ζ_A, T_A) , it is assumed that until the temperature is cooled to a temperature lower than M_s , there will be no new martensite phase and the transformation from M_s to M_f is described as

$$\zeta = \frac{1-\zeta_A}{2} [\cos(a_M [T - M_f]) + \frac{1+\zeta_A}{2}] \dots \dots \dots (4.14)$$

Using the above equations, the change in martensite fraction as a function of temperature under free stress condition can be plotted using MATLAB as shown in Figure 4.2 , see AppendixA, and Appendix B

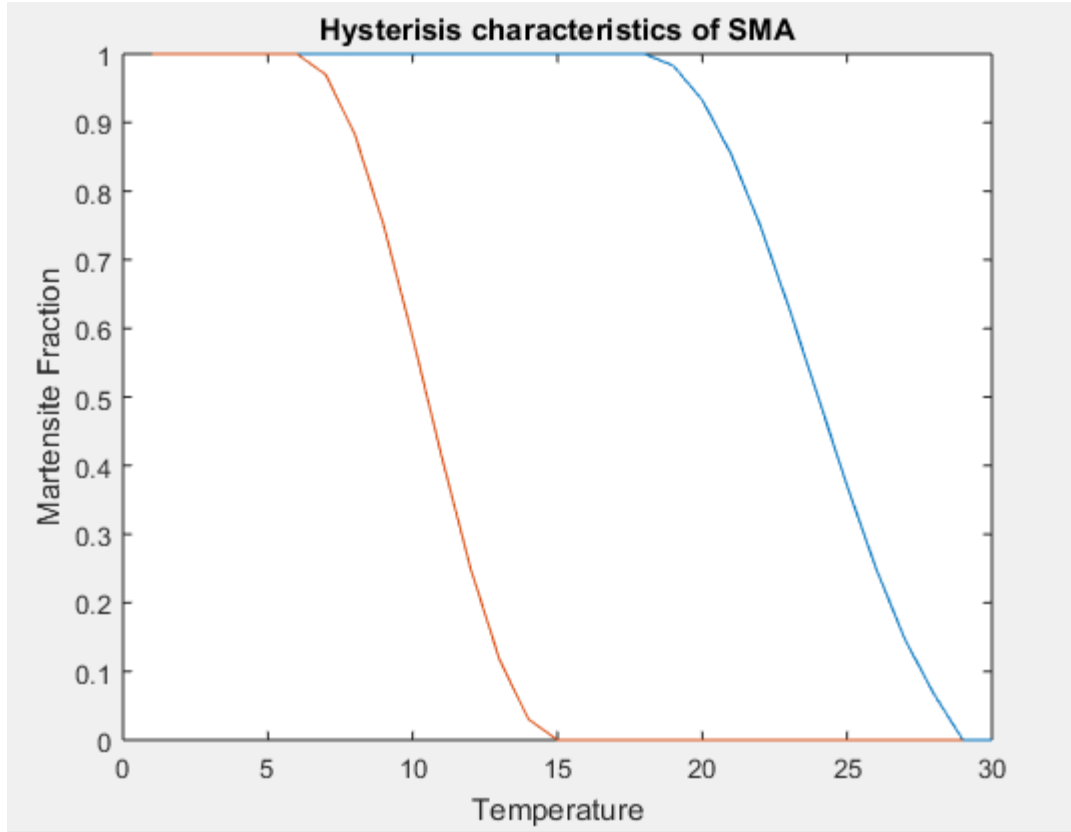


Figure 23: Martensite Fraction vs Temperature

The SMA model used in the simulation for the controller design is derived by Jayender using Liang’s model. This particular model was chosen due to excellent tracking response in the simulation and experimental results which clearly justify the use of the model for describing the transformation between martensite and austenite phases. This model replicates the behaviour of the SMA on the physical process involved. Due to the occurrence of hysteresis, the modelling of heating and cooling of the SMA actuator were separated.[5]

This model consists of three dynamic equations describing the variation of mole fraction with temperature using Fermi–Dirac statistics, temperature dynamics based on Joules heating—convictional cooling, a constitutive equation relating the stress and strain in SMA to changes in temperature and the mole fraction of the SMA in the austenite phase given as

$$\sigma = E\varepsilon - \theta_T T + \Omega \zeta \dots\dots\dots (4.15)$$

where σ is the stress in the SMA, E is the Young's modulus of the alloy, ε is the strain, θ_t is the thermal expansion factor, $\Omega = -E\varepsilon_i$ is the phase transformation contribution factor, and ε_i is the initial strain the SMA.

The dynamic characteristics of the SMA are completely defined by either heating or cooling. σ_e can be defined as the integral of the error.

$$\sigma_\varepsilon = \varepsilon - \varepsilon_{\text{ref}} \dots\dots\dots (4.16)$$

Where ε_{ref} is the reference trajectory. The dynamic equations of the SMA along with equation (4.16) can be represented in the state-space form

$$\dot{Z} = [z, u, t] \dots\dots\dots (4.17)$$

Where

$$\dot{Z} = [\varepsilon \ T \ \zeta \ \sigma_\varepsilon]^T$$

And u is the input voltage to the SMA wire. The nonlinear equations are linearized about a set of operating points $(\varepsilon_o, T_o, \zeta_o, u_o)$ on the reference trajectory.

Equation (4.15) is linearized about the calculated operating points, assuming the no-load case, to obtain linear models in the form

$$\dot{Z} = AZ + Bu, \quad y = CZ \dots\dots\dots (4.18)$$

Where

$$A = \left[\frac{\partial f}{\partial z} \right]_{\varepsilon_o, T_o, \zeta_o, u_o} \quad B = \left[\frac{\partial f}{\partial u} \right]_{\varepsilon_o, T_o, \zeta_o, u_o}$$

The closed form expressions of A and B are given as

$$A = \begin{bmatrix} 0 & \frac{1}{D} H_{func}(-\theta_T - \Omega G_{func}) & 0 & 0 \\ 0 & H_{func} & 0 & 0 \\ 0 & H_{func} G_{func} & 0 & 0 \\ 1 & 0 & 0 & 0 \end{bmatrix}$$

$$B = \begin{bmatrix} \frac{2u}{mc_p R D} (-\theta_T - \Omega G_{func}) \\ \frac{2u}{mc_p R} \\ \frac{2u}{mc_p} G_{func} \\ 0 \end{bmatrix}$$

Where

$$H_{func} = \frac{-hA - 2h_2AT(T - T_a)}{mc_p} \dots\dots\dots (4.19)$$

$$G_{func} = \frac{k \exp\left(\frac{T_f - T}{\sigma_i}\right)}{\sigma_i \left(1 + \exp\left(\frac{T_f - T}{\sigma_i}\right)\right)^2} \dots\dots\dots (4.20)$$

Where T_f is chosen either as A_f or M_f according to whether the SMA actuator is being heated or cooled. Correspondingly, σ_i is chosen as either σ_a or σ_m and K is chosen as ζ_A or ζ_M .

4.5 Control formula and Simulation approach

Precise shape of control is difficult to define due to the nonlinearities, slow response of the SMA actuators and the low heat endurance tolerance of ABS, the best controller for this system, it seems to be the PID controller as a good starting point. The PID controller is the most common form of feedback with 76 more than 95% of the control loops in process control being of PID type, where most loops are actually PI control [7]

The controller regulates the electric current of the actuators to reach the desired shape of the airfoil. The input of the control system is $S_{ref}(t)$ which is the reference value for the morphing of the wing. $S(t)$ is the actual output of the control system, e is the control error and corresponds to the difference between $S(t)$ and $S_{ref}(t)$. Since we consider a regulator problem $S_{ref}(t) = 0$, Therefore $e = s$, control structure is shown in the block diagram

Figure 24

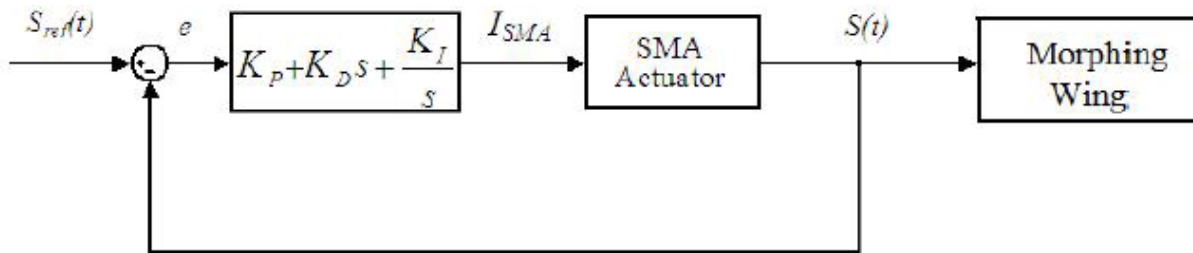


Figure 24: Block diagram of the system under consideration

The input of the control system is $S_{ref}(t)$ which is the reference value for the morphing of the wing. $S(t)$ is the actual output of the control system, e is the control error and corresponds to the difference between $S(t)$ and $S_{ref}(t)$.

If the control error $e = S_{ref}(t) - S(t)$ is positive, that is, the strain of the actual wing deflection $S(t)$ is smaller than the desired strain, $S_{ref}(t)$, the controller generates a signal I_{SMA} which turns the actuator on, allowing electrical current to flow through the SMA wire. The temperature of the wire then starts to increase due to the Joule effect produced by the electrical current. As the martensite to austenite phase transformation start temperature A_s is reached, the wire starts to recover its high-temperature shape (shorter

length), generating a force and creating a moment which deflects the wing until it reaches the reference value $S_{ref}(t)$. On the other hand, if e is negative, the strain on the upper surface of the wing, $S(t)$, is larger than the desired strain, $S_{ref}(t)$, the controller turns the actuator off by cutting the electrical current so that the actuator is cooled by the surrounding air.

PID controller is able to take a time derivative or time integral of the input signal, in addition to proportional operation. In designing a controller, it is crucial to determine which of these components should be used, in what proportion and how they are related. The transfer function of the basic PID controller is given by

$$G_c(s) = K_p + K_D s + \frac{K_I}{s} \dots\dots\dots (4.21)$$

Where K_P , K_D , and K_I are real constants. For the application in a morphing wing, it involves the determination of the values of these three constants so that the performance of the system meets the design requirements, PID controller block is shown below, figure

25

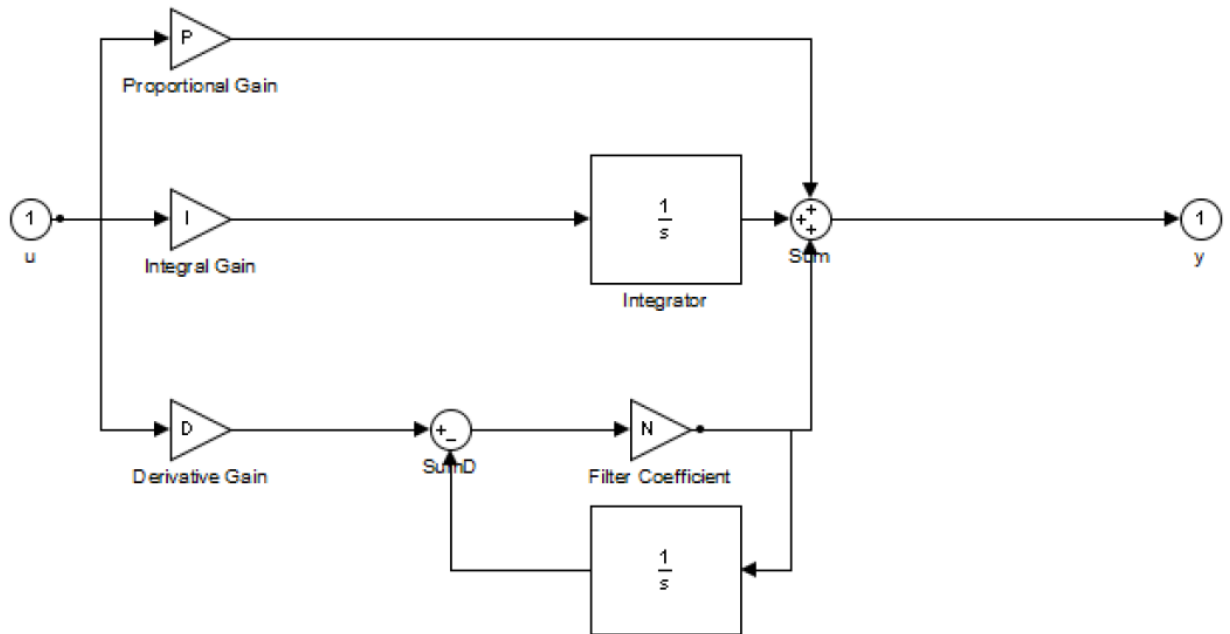


Figure 25: PID Controller block of morphing trailing edge

Simulation is carried out by adding the mathematical model which is calculated by the means of Liang & Rogers' and executed in a Matlab code Appendix B to the PID controller, which is fed to a step input, the output is fed back with a unity feedback to the controller, see figure 26

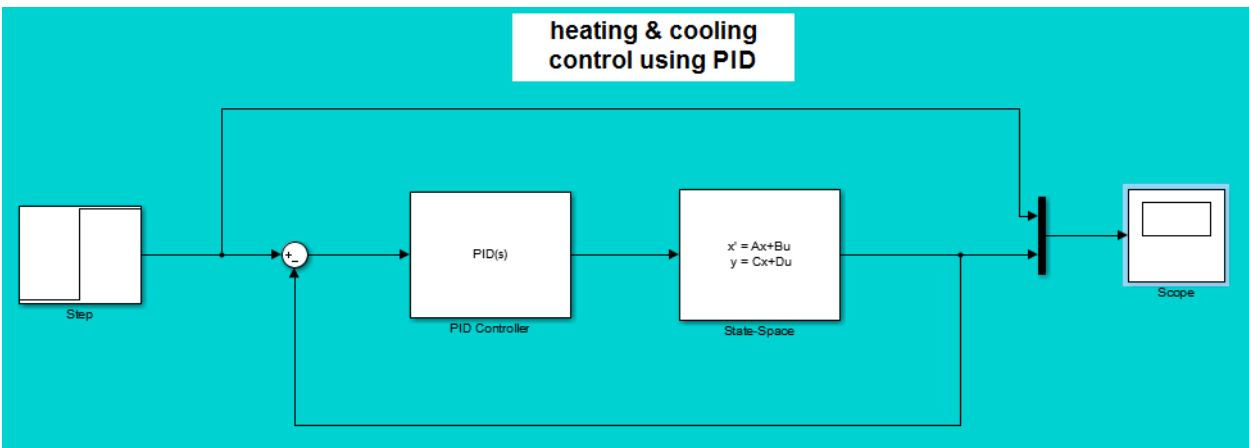


Figure 26: Simulation scheme

Chapter 5: Result And Discussion

5.1 Result Demonstration and Assessment

Control experiment separated into two approaches the heating model and the cooling model.

- **outcomes of the heating model**

after applying the PID controller to the dynamic characteristic of the SMA which is explained in a matlab code in appendix B, figure (27) show the time response with I Controller ,which seems to be the best controller type, Characteristic and controller Parameters are shown in table 9 below, and Scope shows figure(28).

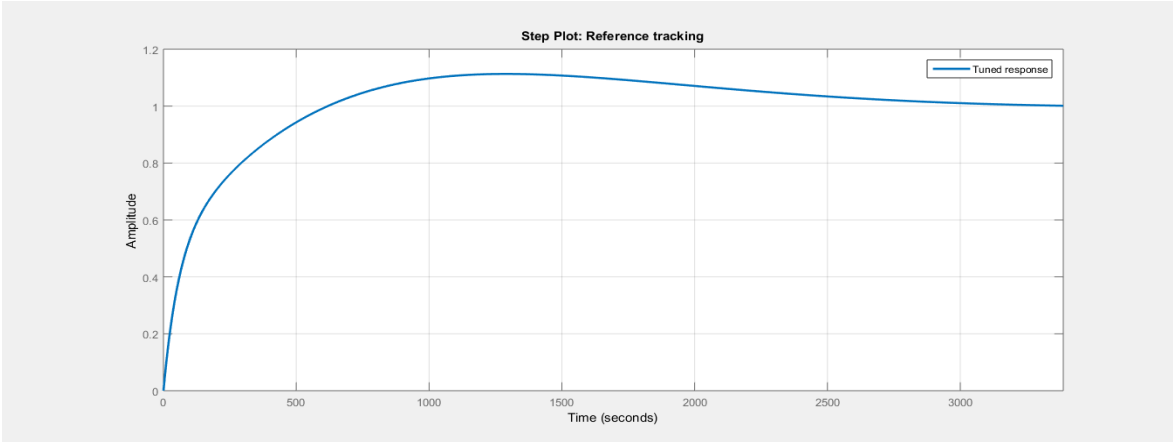


Figure 27: The time response with I Controller for heating

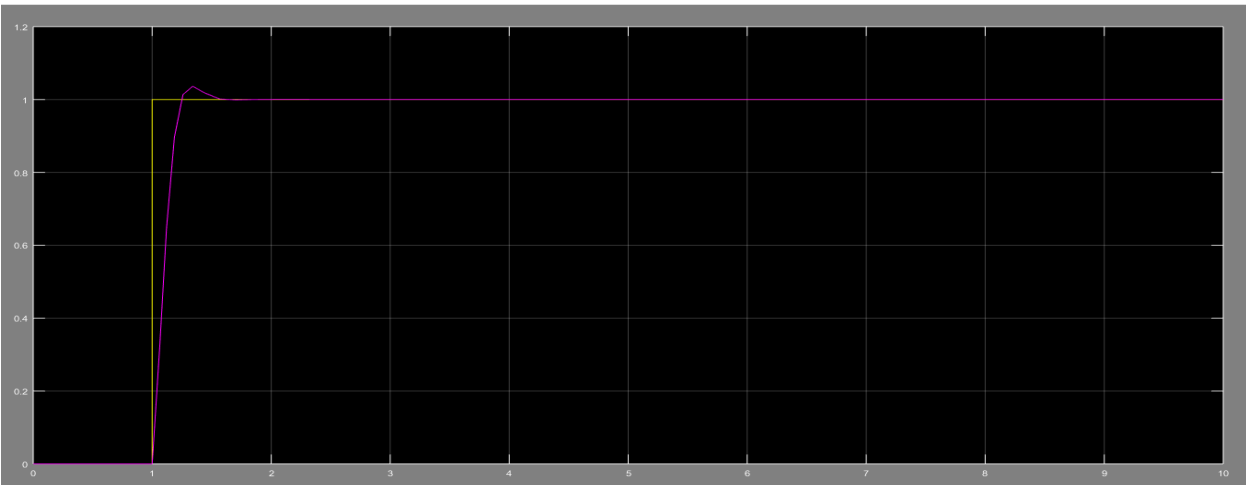
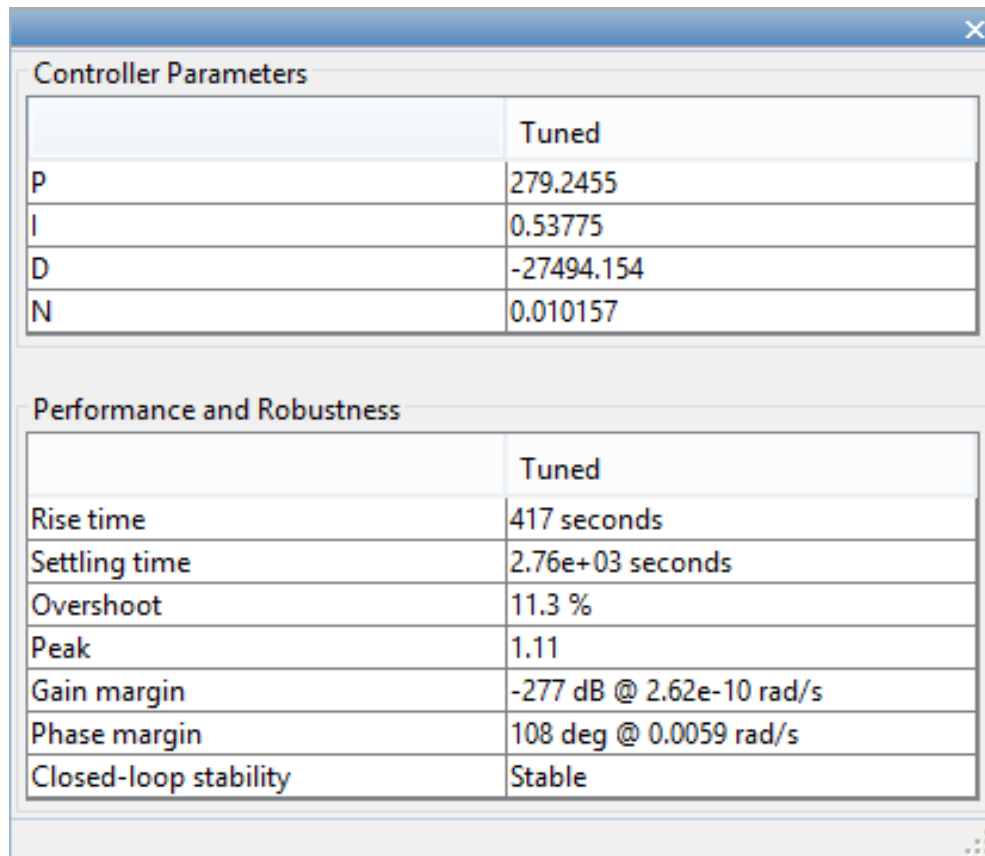


Figure 28: Scope Result for heating

Table 9: Characteristic and controller Parameters for heating



Controller Parameters	
	Tuned
P	279.2455
I	0.53775
D	-27494.154
N	0.010157

Performance and Robustness	
	Tuned
Rise time	417 seconds
Settling time	2.76e+03 seconds
Overshoot	11.3 %
Peak	1.11
Gain margin	-277 dB @ 2.62e-10 rad/s
Phase margin	108 deg @ 0.0059 rad/s
Closed-loop stability	Stable

- **outcomes of the cooling model**

after applying the PID controller to the dynamic characteristic of the SMA which is explained in a matlab code in appendix B, figure 29 show the time response with I Controller ,which seems to be the best controller type, Characteristic and controller Parameters are shown in table 10 below, and Scope shows figure (30).

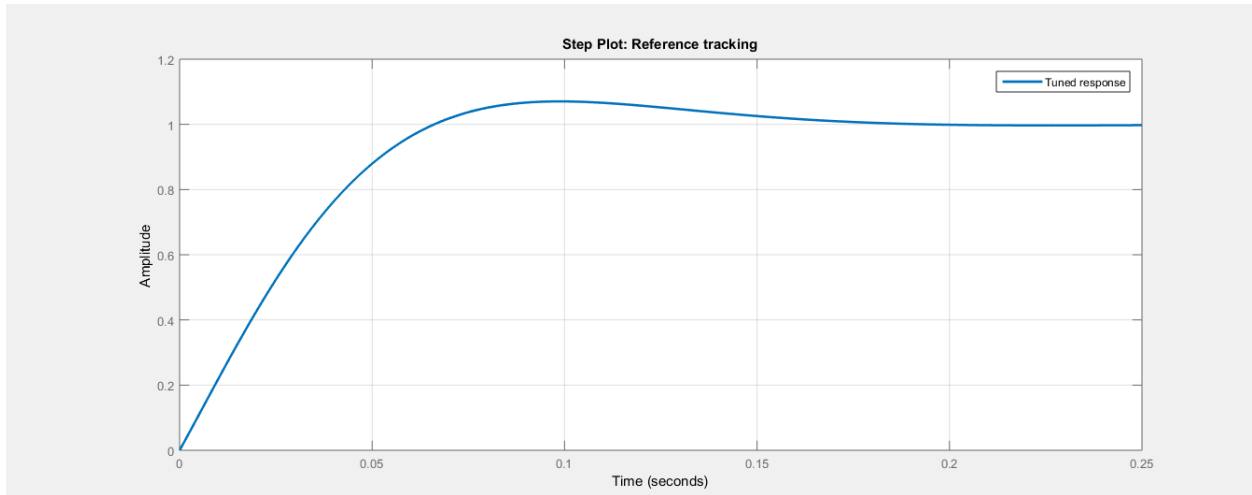
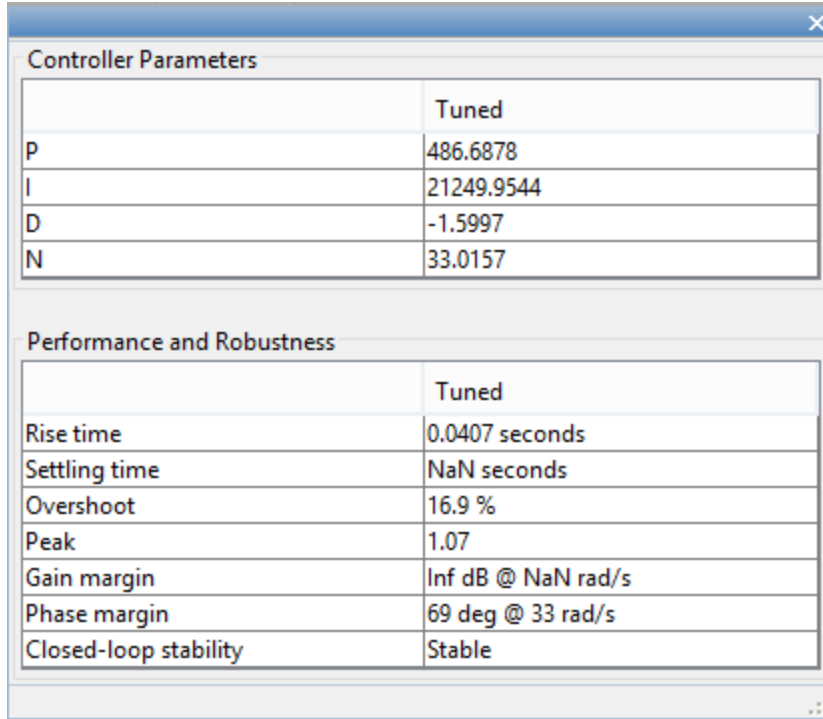


Figure 29: The time response with I Controller for cooling



Figure 30: Scope Result for cooling

Table 10: Characteristic and controller Parameters for cooling



Controller Parameters	
	Tuned
P	486.6878
I	21249.9544
D	-1.5997
N	33.0157

Performance and Robustness	
	Tuned
Rise time	0.0407 seconds
Settling time	NaN seconds
Overshoot	16.9 %
Peak	1.07
Gain margin	Inf dB @ NaN rad/s
Phase margin	69 deg @ 33 rad/s
Closed-loop stability	Stable

5.2 Evaluation Result

Despite of the fact that the cooling action is more complicated and has a slow response due to the natural heat convection ,the controller shows better performance for the cooling action than the heating control action, which is completely a conflict consequence, the system has a stable behavior for both heating and cooling model with reasonable robustness.

For the heating model the amplitude increases with time until it reaches its settling time and then it becomes stable (fig (27)), the rise time is (417s) , settling time is (2.76e+0.3s), the overshoot is (11.3%) and peak equal (1.11).

For cooling model in fig (29) the rise time decreased to (0.0407s), the settling time turned to NaN second, the overshoot increased to (16.9%) and the peak is 1.07.

Chapter 6: Conclusion And Recommendations

6.1 Conclusion:

In the studying of smart materials, their properties in response to external condition such as temperature, stress, electrical charge, magnetic field, are understood and these unique properties receive a great attention from the airspace industry. The reason is that properties can be applied to different parts in the aircraft to improve the overall performance. For example, by using the smart material actuator, its performance is much more efficient than the conventional system since the electricity is directly converse to actuation, numbers of parts are greatly reduced and transmitting speed of electricity is much higher. Moreover, an innovative research is experiencing to make the adaptive wing or control surfaces which can greatly increase the maneuverability.

In addition, smart material is usually light in weight and can be made in the compact size. At the same time, cost can be reduced and maintenance can be minimized by using vibration control smart material. Accordingly, the demand of smart structure constructed by smart materials is increase dramatically because it can improve the overall efficiency, maneuverability, safety, stability, light weighted structure of the aircrafts.

PID control is easy to be implemented as it is well-known to all control engineers and there are numerous techniques to tune the controller, either through experiments or theoretically.

The control and validation results for an actuation system of a morphing trailing edge were exposed by using developed morphing mechanism used smart materials such as Shape Memory Alloy (SMA). Two architectures were developed for controlling the system for heating model and cooling model, the modeled system has reasonable robustness, the stability and the whole actuation system has accomplished its purpose.

6.2 Recommendation:

The most obvious note is that the rate of cooling is very slow which consequently affected the performance of the actuators, so cooling device must be added.

The performance of the SMA actuator is altered considerably if the surface to volume ratio is changed because the bandwidth of a SMA wire is mainly determined by heat transfer through the surface of the wire. So it is better to use many thin wires instead of a single thick wire to improve the force capabilities of an SMA actuator without affecting the bandwidth. The wires must also remain separated to ensure effective cooling by allowing air to flow freely around all surfaces.

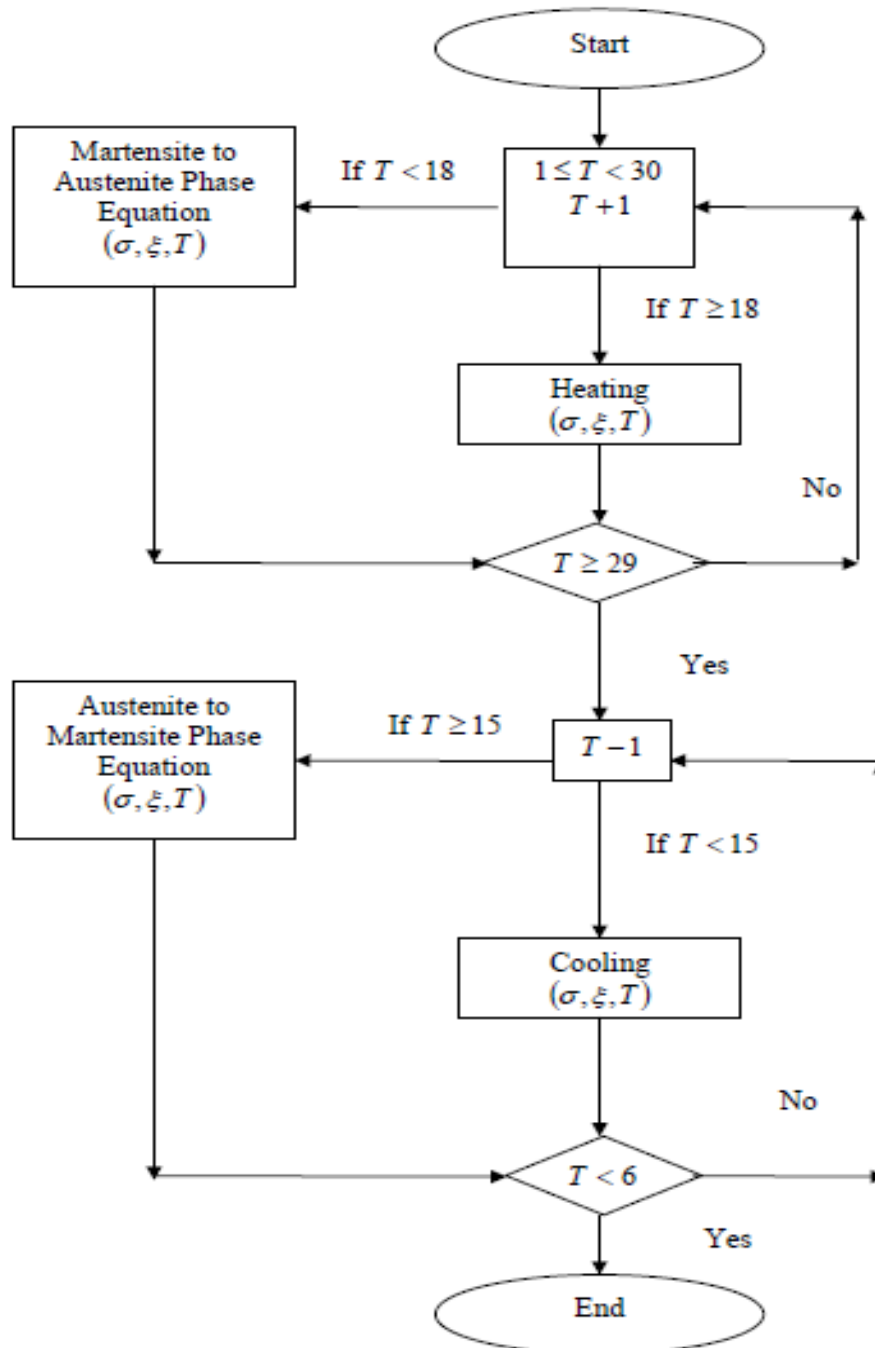
6.3 Future work:

Due to the strong non-linear character of the smart materials actuators used in our application, it is difficult to precisely describe the controlled system by conventional mathematical relations, simplicity and flexibility capabilities offered by the fuzzy logic techniques make them more practical due to their closeness to human perception and reasoning, future work is to work on improve the control model by using fuzzy logic controller (FLC).

References

- [1] ROTH, B.D. and CROSSLEY, W.A. Applications of optimization techniques in the conceptual design of morphing aircraft 2003, Third Annual Aviation Technology, Integration, and Operations (ATIO), Denver, CO, USA.
- [2] BARTLEY-CHO, J.D., WANG, D.P., MARTIN, C.A., KUDVA, J.N. and WEST, M.N. Development of high-rate, adaptive trailing edge control surface for the smart wing phase 2 wind tunnel model, *J Intell Mat Sys and Struc*, 2004, 15, (4), pp 279-291.
- [3] Arrison, L., Birocco, K., Gaylord, C., Herndon, B., Manion, K., Metheny, M., "2002-2003 AE/ME Morphing Engineering Department, Virginia Polytechnic Institute and State University, May 2003.
- [4] Raymer, D., "Vehicle Scaling Laws for Multidisciplinary Optimization," AIAA 01-0532, 39th AIAA Aerospace Sciences Meeting, Reno, NV, Jan 2001.
- [5] Kinzel M.P., Maughmer M.D., Lesieutre G.A., 2007, "Miniature Trailing-Edge Effectors for Rotorcraft Performance Enhancements", *J. of the American Helicopter Society*, Vol.52, No.2, pp. 146-158
- [6] Sofla A. Y. N., Elzey D. M., Wadley H. N. G., "Two-way Antagonistic Shape Actuation Based on the One-way Shape Memory Effect.," *Journal of Intelligent Material System Structure*, Vol. 19, pp.1017-27, 2008
- [7] Asua E., Etxebarria V. and Garcia-Arribas A., "Neural Network-Based Micro Positioning Control of Shape Memory Alloy Actuators," *Engineering Applications of Artificial Intelligence*, Vol. 21. No. 5, 2008.
- [8] Popov A. V., Labib M., Fays J., and Botez R. M., "Closed-Loop Control Simulations on a Morphing Wing," *Journal of Aircraft*, Vol. 45, No. 5, pp. 1794-1803, 2008.
- [9] Song G., Ma N., 2007, "Robust control of a shape memory alloy wire actuated flap", *Smart Materials and Structures*, Vol.16, pp. N51-N57

Appendix A: Flowchart of the Heating and Cooling of SMA



Appendix B: MATLAB M-File

MATLAB M-File for Modelling Martensite Fraction for SMA

```
u = 2;
m = 4.54*exp(-4);
cp = 320;
R = 13.0677;
Da = 75*exp(9);
Dm = 28*exp(9);
theta_t = -11*exp(-6);
epsilon_i = 0.03090;
h0 = 28.552;
h2 = 4.060*exp(-6);
d = 304*exp(-6);
l = 0.24;
Ta = 20;
Tfa = 85;
Tfm = 42;
sigma_a = 6;
sigma_m = 4.5;
zita_1 = 1;
zita_2 = 0;
As = 18;
Af = 30;
Ms = 15;
Mf = 6;
aA = pi/(Af-As);
aM = pi/(Ms-Mf);
temp = [];
zita = [];
for i=1:30
    if i <= 18
        state = 1;
    elseif i >18 & i < 29
        state = 2;
    else i >= 29
        state = 3
    end
    if state == 1
        K = zita_1;
    elseif state == 2
        zita_i = 0.5*(cos(aA*(i-As))+1);
        K = zita_i;
    elseif state == 3
        K = zita_2;
    else state == 4
        zita_i = 0.5*(cos(aM*(i-Mf))+1);
        K = zita_i;
    end
end
```

```

temp(i) = i;
zita(i) = K;
end
plot(temp,zita)
hold on
temp = [];
zita = [];
for j=1:29
if j >= 15,
state = 3
elseif j < 15 & j > 6
state = 4
else j <= 6
state = 1
end
if state == 1
K = zita_1;
elseif state == 2
zita_i = 0.5*(cos(aA*(j-As))+1);
K = zita_j;
elseif state == 3
K = zita_2;
else state == 4
zita_i = 0.5*(cos(aM*(j-Mf))+1);
K = zita_i;
end
temp(j) = j
zita(j) = K
end
plot(temp,zita)
hold off
title('Hysteresis characteristics of SMA')
xlabel ('Temperature')
ylabel ('Martensite Fraction')

```


MATLAB M-File for Modelling the Heating Function for SMA

```
t=10
x=3;
%u=10;
flag=3;
T = 1; % Start temperature
% while T < 29
if T < 18
state = 1;
else T >= 18
state = 2;
end
v = 2; % input voltage
m = 4.54*exp(-4); % mass per unit length
cp = 320; % specific heat capacity
R = 3.05; % resistance per unit length
Da = 75*exp(9); % Young's Modulus (Austenite)
Dm = 28*exp(9); % Young's Modulus (Martensite)
theta_t = -11*exp(-6); % Thermal expansion
epsilon_i = 0.03090; % SMA initial strain
h0 = 28.552; % Heat convection coefficient
h2 = 4.060*exp(-6); % Heat convection coefficient
d = 1220*exp(-6); % Diameter of wire
l = 0.035; % Length of wire
Ta = -13; % Ambient temperature
Tfa = 70; % Martensite to austenite transformation temperature
Tfm = 55; % Austenite to martensite transformation temperature
sigma_a = 6; % Spread of temperature around martensite to austenite
transformation temperature
sigma_m = 4.5; % Spread of temperature around martensite to austenite
transformation temperature
zita_1 = 1;
zita_2 = 0;
As = 18;
Af = 30;
Ms = 15;
Mf = 6;
aA = pi/(Af-As);
aM = pi/(Ms-Mf);
if state == 1;
D = Dm;
K = zita_1;
sigma_i = sigma_m;
Tf = Tfm;
elseif state == 2;
zita_i = 0.5*(cos(aA*(T-As))+1);
sigma_i = sigma_m;
D = Dm;
K = zita_i;
```

```

Tf = Tfm;
elseif state == 3;
D = Da;
K = zita_2;
sigma_i = sigma_a;
Tf = Tfa;
else state == 4;
zita_i = 0.5*(cos(aM*(T-Mf))+1);
sigma_i = sigma_a;
D = Da;
K = zita_i;
Tf = Tfa;
end
a = pi*d;
h = h0+h2*T^2;
Ohm = -D*epsilon_i;
Hfunc = (-h*a-2*h2*a*T*(T-Ta))/(m*cp);
Gfunc = (K*exp((Tf-T)/sigma_i))/(sigma_i*(1+exp((Tf-T)/sigma_i))^2);
A = [ 0 1/D*Hfunc*(-theta_t-Ohm*Gfunc) 0 0
0 Hfunc 0 0
0 Hfunc*Gfunc 0 0
1 0 0 0 ]
B = [ 2*v/(m*cp*R*D)*(-theta_t-Ohm*Gfunc)
2*v/(m*cp*R)
2*v/(m*cp)*Gfunc
0 ]
%T = T+1;
C = [1 1 1 1 ]
D = [0]

```

MATLAB M-File for Modelling the Cooling Function for SMA

```
t=10
x=3;
%u=10;
flag=3;
T = 30; % Start temperature
%while T > 1
if T >= 15,
state = 3;
elseif T < 15 && T > 6
state = 4;
else
state = 1;
end
v = 2; % input voltage
m = 4.54*exp(-4); % mass per unit length
cp = 320; % specific heat capacity
R = 3.05; % resistance per unit length
Da = 75*exp(9); % Young's Modulus (Austenite)
Dm = 28*exp(9); % Young's Modulus (Martensite)
theta_t = -11*exp(-6); % Thermal expansion
epsilon_i = 0.03090; % SMA initial strain
h0 = 28.552; % Heat convection coefficient
h2 = 4.060*exp(-6); % Heat convection coefficient
d = 1220*exp(-6); % Diameter of wire
l = 0.035; % Length of wire
Ta = -13; % Ambient temperature
Tfa = 70; % Martensite to austenite transformation temperature
Tfm = 55; % Austenite to martensite transformation temperature
sigma_a = 6; % Spread of temperature around martensite to austenite
transformation temperature
sigma_m = 4.5; % Spread of temperature around martensite to austenite
transformation temperature
zita_1 = 1;
zita_2 = 0;
As = 18;
Af = 30;
Ms = 15;
Mf = 6;
aA = pi/(Af-As);
aM = pi/(Ms-Mf);
if state == 1;
zita_i = zita_1;
D = Dm;
K = zita_i;
sigma_i = sigma_m;
Tf = Tfm;
elseif state == 2;
zita_i = 0.5*(cos(aA*(T-As))+1);
```

```

sigma_i = sigma_m;
D = Dm;
K = zita_i;
Tf = Tfm;
elseif state == 3;
zita_i = zita_2;
D = Da;
K = zita_i;
sigma_i = sigma_a;
Tf = Tfa;
else
zita_i = 0.5*(cos(aM*(T-Mf))+1);
sigma_i = sigma_a;
D = Da;
K = zita_i;
Tf = Tfa;
end
a = pi*d;
h = h0+h2*T^2;
Ohm = -D*epsilon_i;
Hfunc = (-h*a-2*h2*a*T*(T-Ta))/(m*cp);
Gfunc = (K*exp((Tf-T)/sigma_i))/(sigma_i*(1+exp((Tf-T)/sigma_i))^2);
A = [ 0 1/D*Hfunc*(-theta_t-Ohm*Gfunc) 0 0
0 Hfunc 0 0
0 Hfunc*Gfunc 0 0
1 0 0 0 ]
B = [ 2*v/(m*cp*R*D)*(-theta_t-Ohm*Gfunc)
2*v/(m*cp*R)
2*v/(m*cp)*Gfunc
0 ]
%T = T - 1;
C = [1 1 1 1]
D = [0]

```